Multidimensional Imaging in Service of Plant Phenotyping

Ladislav Nedbal

nedbal.lad@gmail.com

EPPN Summer School, Szeged, Hungary / July 3rd 2013

Multidimensional Imaging

Phenotyping ≈ "… set of methodologies and protocols used to measure plant growth, architecture, and composition …, from organs to canopies."

Fiorani and Schurr (2013) Annu. Rev. Plant Biol.64:17.1–17.25

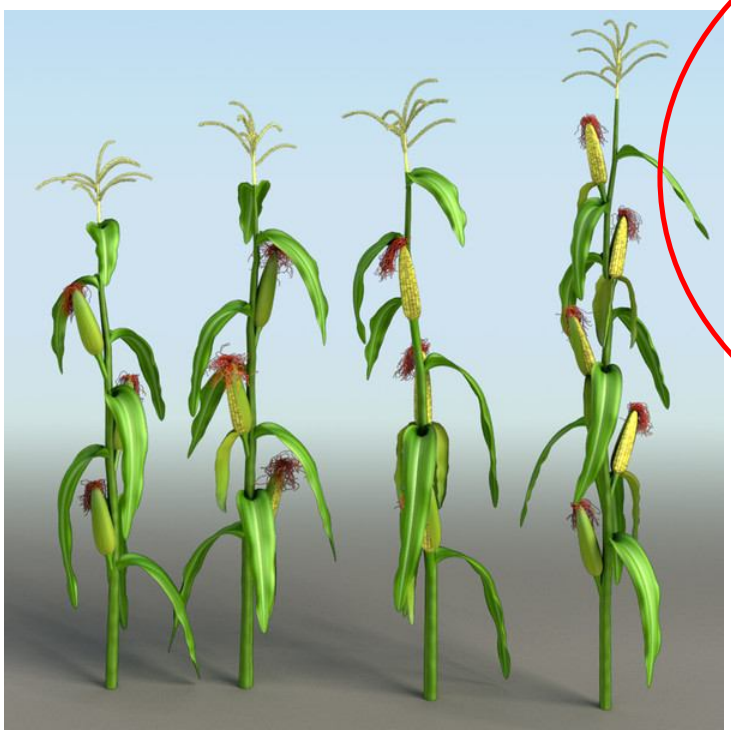

3D (cm x cm x cm)

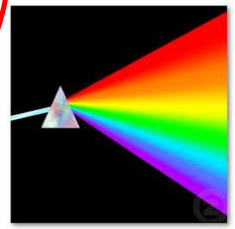

+ 1D [λ nm]

+ 1D [days]

…… more?

1. Plant 3-D reconstruction
2. Adding Chl-fluorescence in time to 5-D
3. Statistical feature selection and combinatorial imaging

3D reconstruction

Passive methods– stereo imaging

– space carving

3D (cm x cm x cm)

Active methods – laser light detection and ranging, LIDAR

– structured light

Space carving

Overview

LemnaTec
www.lemnatec.com

- Algorithm idea
- Hardware requirements
- Results
- Future developments

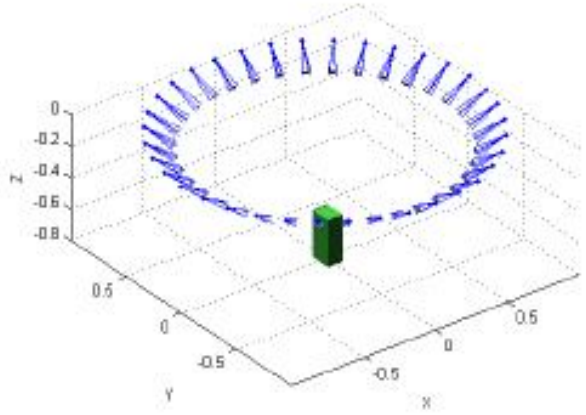

Speaker: Dirk Vandenhirtz, Stefan Schwartz Date: 8/29/2011 Slide 2

http://www.lemnatec.com/sites/default/files/application-sheets/2011/08/29/3D.pdf

Space carving

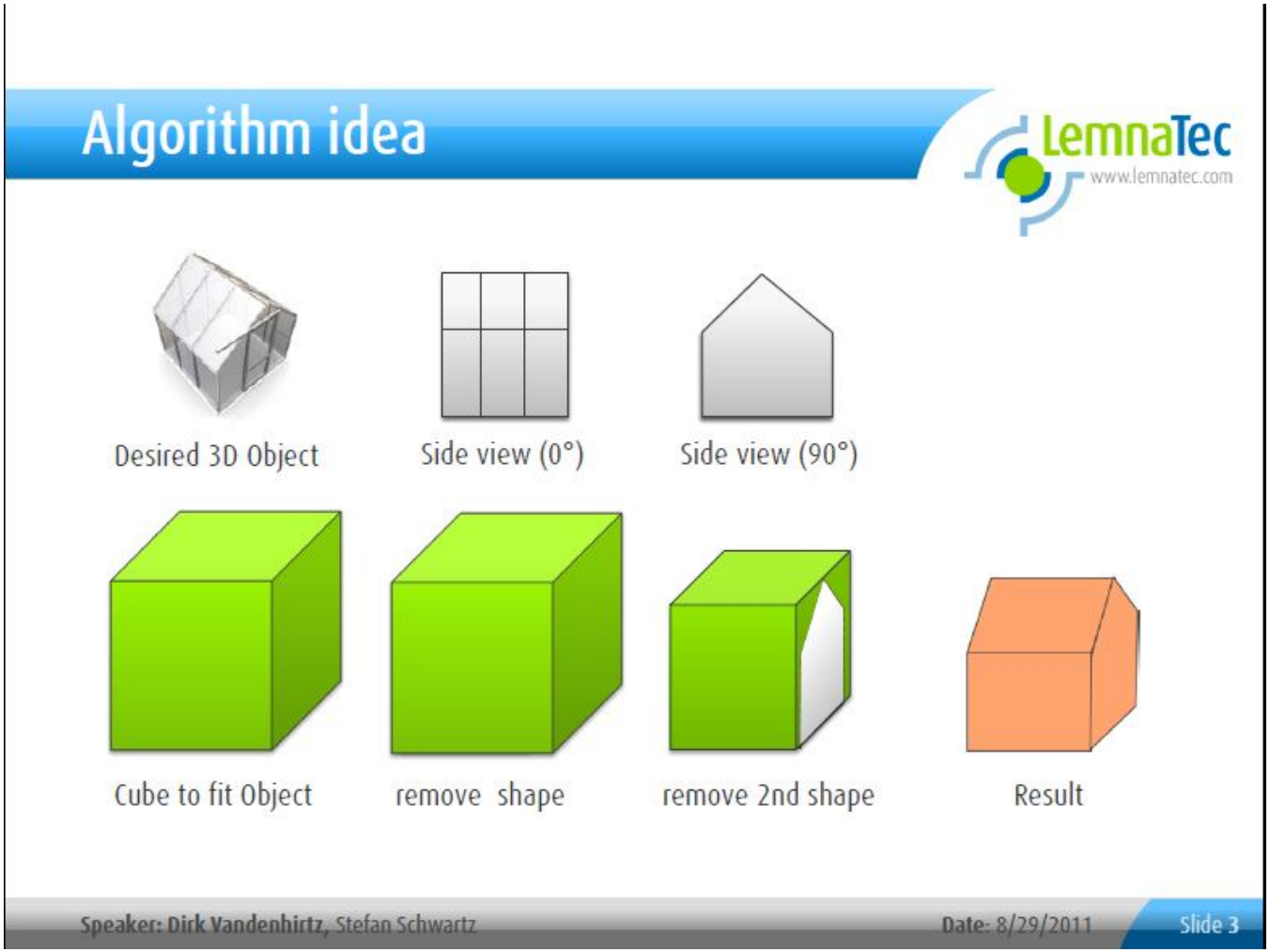

http://www.lemnatec.com/sites/default/files/application-sheets/2011/08/29/3D.pdf

3D reconstruction

Passive methods– stereo imaging

– space carving

3D (cm x cm x cm)

Active methods – laser light detection and ranging, LIDAR

– structured light

LIDAR (Light Detection and Ranging)

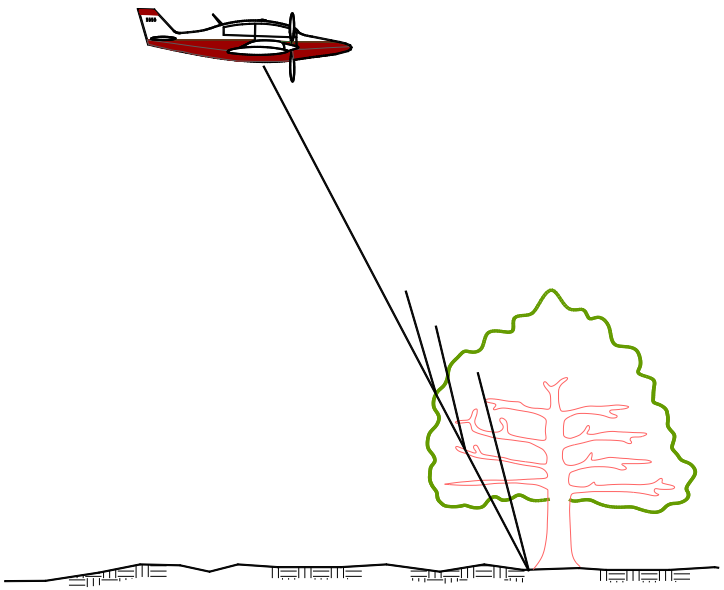

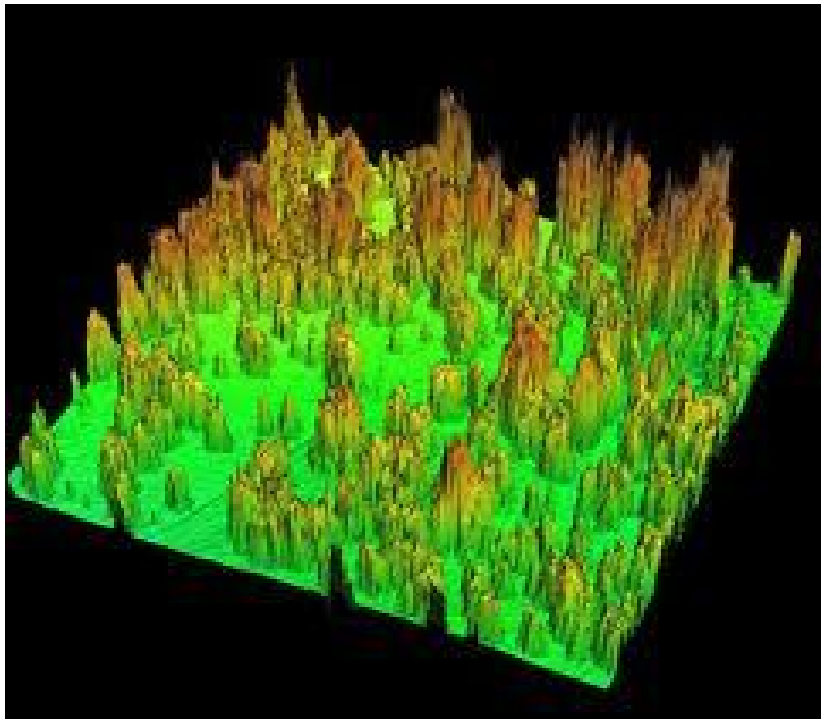

mapwv.gov/wvagp/conference/presentations/Meade.ppt

LIDAR (Light Detection and Ranging)

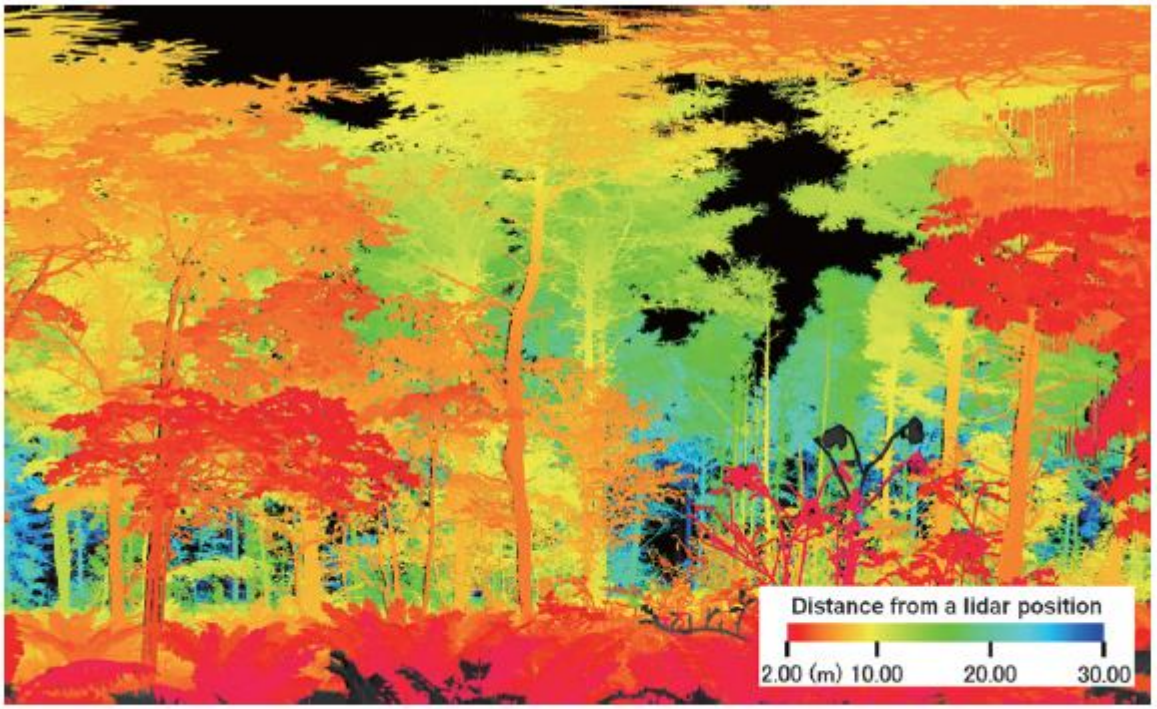

Fig. 8. False-colour image of a Japanese larch (*Larix leptolepis* Gordon) forest measured using a ground-based scanning lidar system with 8 mm range accuracy (Omasa *et al.*, 2002*b*). Numerical values in the colour scale represent the distance from the lidar system.

Omasa K, Urano Y, Oguma H, Fujinuma Y. 2002*b*. Mapping of tree position of *Larix leptolepis* woods and estimation of diameter at breast height (DBH) and biomass of the trees using range data measured by a portable scanning lidar. *Journal of Remote Sensing Society of Japan* **22,** 550–557.

LIDAR (Light Detection and Ranging)

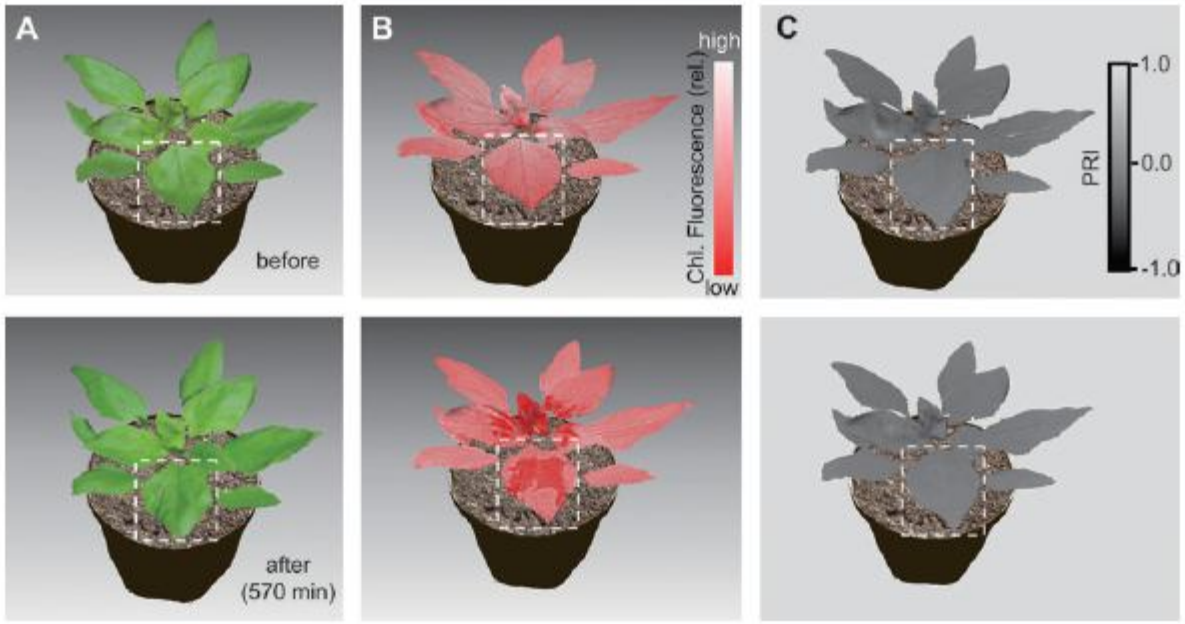

Fig. 12. Changes in 3D composite images of (A) the natural colour of a sunflower (*Helianthus annuus* L.) plant, (B) of chlorophyll (Chl.) *a* fluorescence intensity ('P' at the peak of the Kautsky effect), and (C) of the photochemical reflectance index (PRI) before (top row) and after (bottom row) treatment with glufosinate-ammonium (Basta) herbicide. The original 3D images were measured using an optical probe-based scanning lidar with 0.5 mm range accuracy. The composite images were obtained using a texture-mapping technique that mapped the natural colour, chlorophyll *a* fluorescence intensity, and PRI images to each 3D image. Broken lines show the part of the leaf to which the herbicide was applied. The upper images were measured ~180 min before the herbicide treatment and the lower ones were recorded ~570 min after the treatment. PPFD for fluorescence measurement (Omasa *et al.*, 1987) was 250 μmol m^{-2} s^{-1}. Temperature and relative humidity were 25 °C and 50%, respectively. Growth conditions were the same as those described in Fig. 10.

Kenji Omasa*, Fumiki Hosoi and Atsumi Konishi

Journal of Experimental Botany, Vol. 58, No. 4, pp. 881–898, 2007
Imaging Stress Responses in Plants Special Issue

3D reconstruction

Passive methods – stereo imaging

– space carving

3D (cm x cm x cm)

Active methods – laser light detection and ranging, LIDAR

– structured light

Stereo photograph of a 3D scene

"3D" (cm x cm x cm)

BW

time

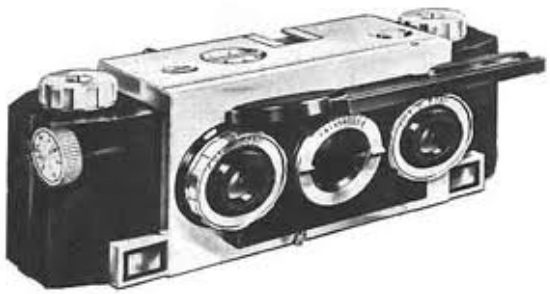

Stereo vision

"3D" (cm x cm x cm)
RGB colors
time

Biskup, B., Scharr, H., Schurr, U., & Rascher, U. (2007).
A stereo imaging system for measuring structural parameters of plant canopies.
Plant Cell and Environment, 30, 1299–1308

Stereo vision

Biskup, B., Scharr, H., Schurr, U., & Rascher, U. (2007).
A stereo imaging system for measuring structural parameters of plant canopies.
Plant Cell and Environment, 30, 1299–1308

Epipolar geometry: geometric relations between 2D images of 3D points photographed by two cameras.

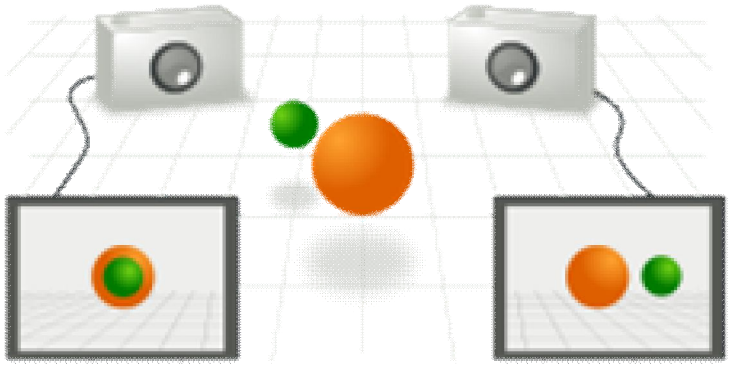

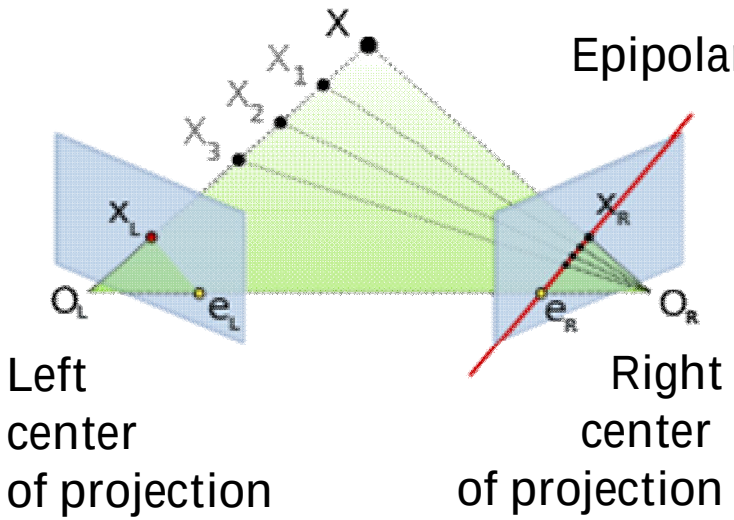

Stereo vision

Biskup, B., Scharr, H., Schurr, U., & Rascher, U. (2007).
A stereo imaging system for measuring structural parameters of plant canopies.
Plant Cell and Environment, 30, 1299–1308

STEP 1: Calibration of cameras

=> focal length, principal point, rad

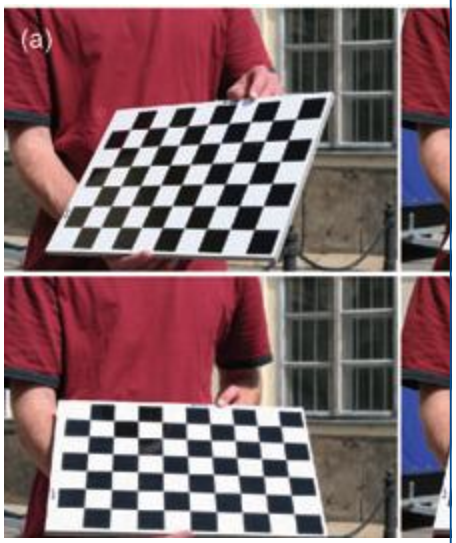

and stereo rig => rotation and trans

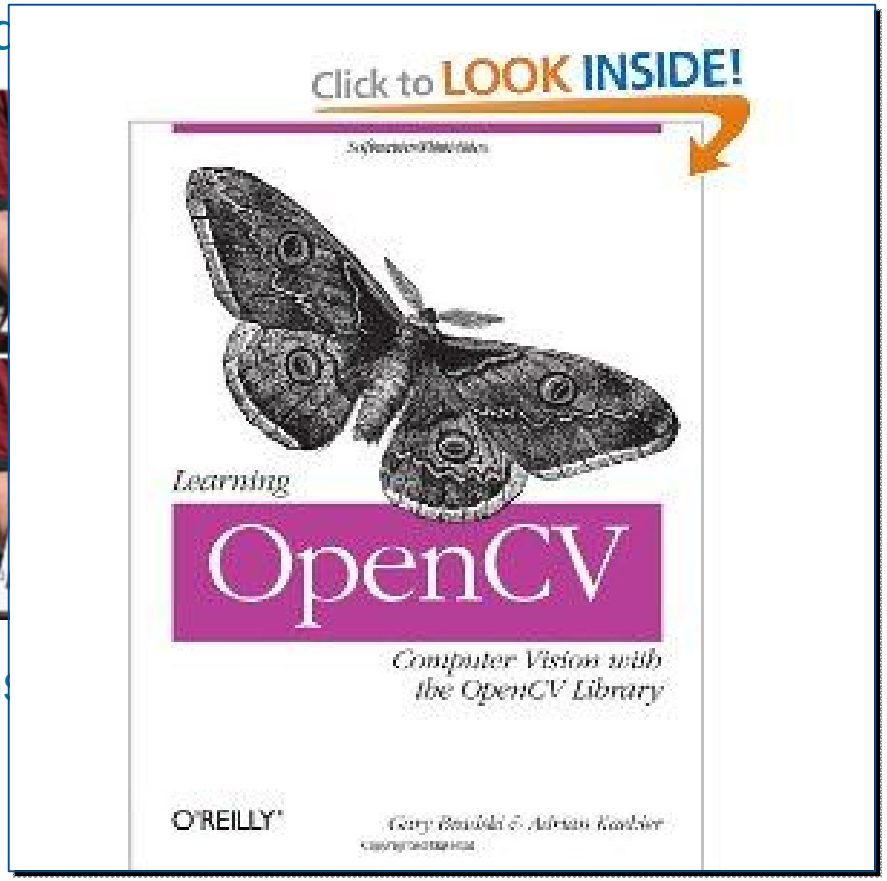

Stereo vision

Biskup, B., Scharr, H., Schurr, U., & Rascher, U. (2007).
A stereo imaging system for measuring structural parameters of plant canopies.
Plant Cell and Environment, 30, 1299–1308

STEP 2: Epipolar Rectification

=> Image transformation alingning epipolar lines and pixel lines

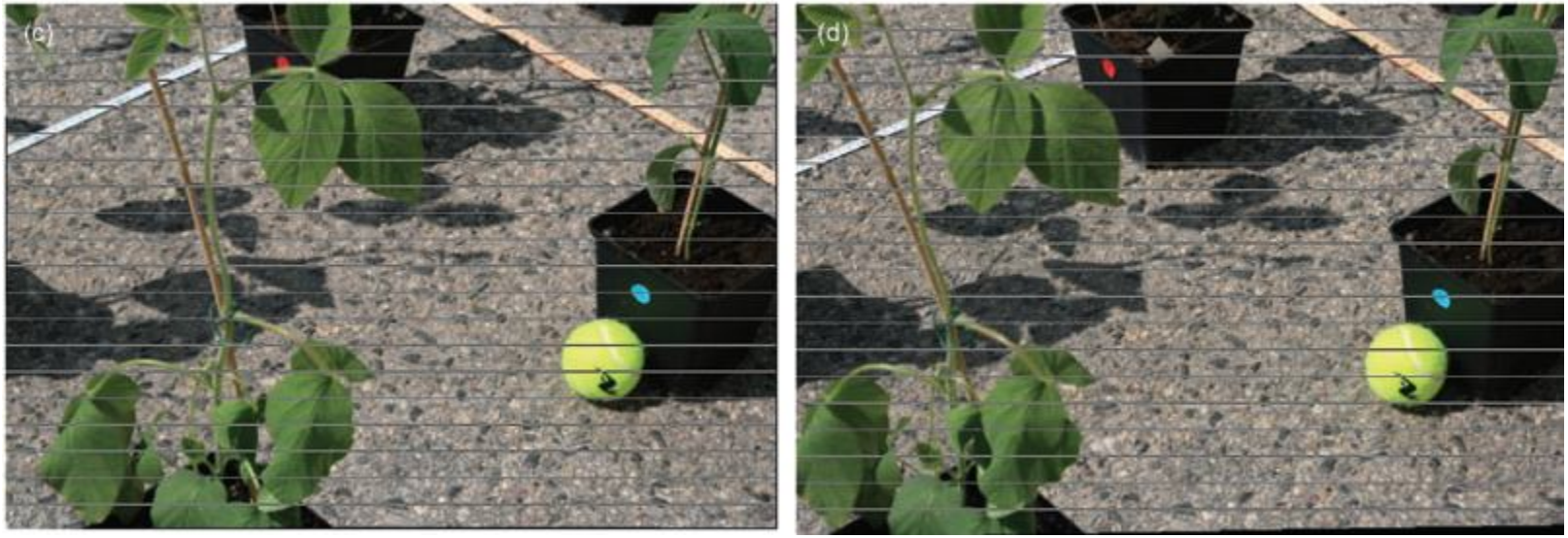

Stereo vision

Biskup, B., Scharr, H., Schurr, U., & Rascher, U. (2007).
A stereo imaging system for measuring structural parameters of plant canopies.
Plant Cell and Environment, 30, 1299–1308

STEP 3: Stereomatching

=> Identification of corresponding points in the 2 images and disparities

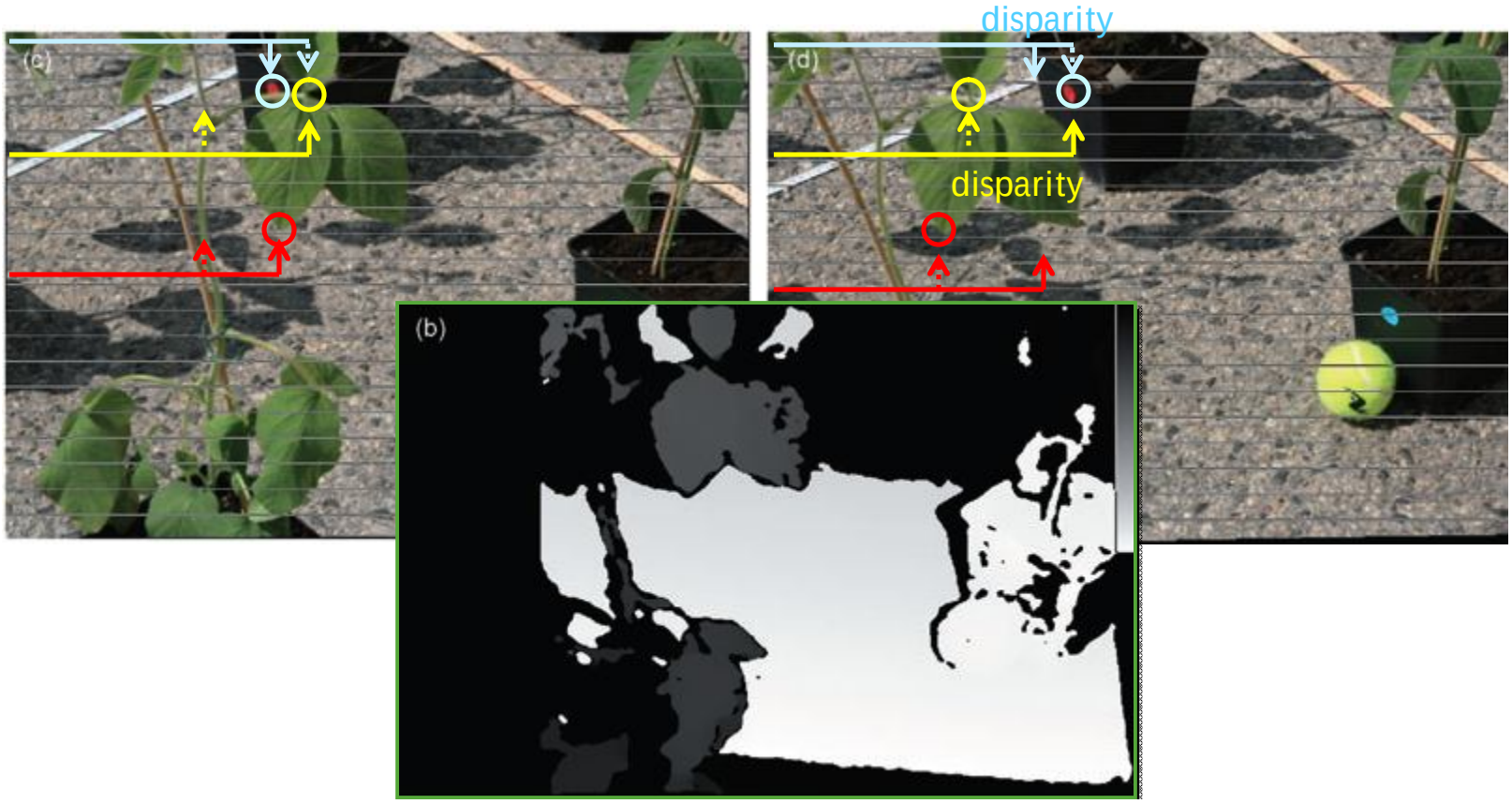

Stereo vision

STEP 4: Image color segmentation

Separating plant image segments, removing background pixels

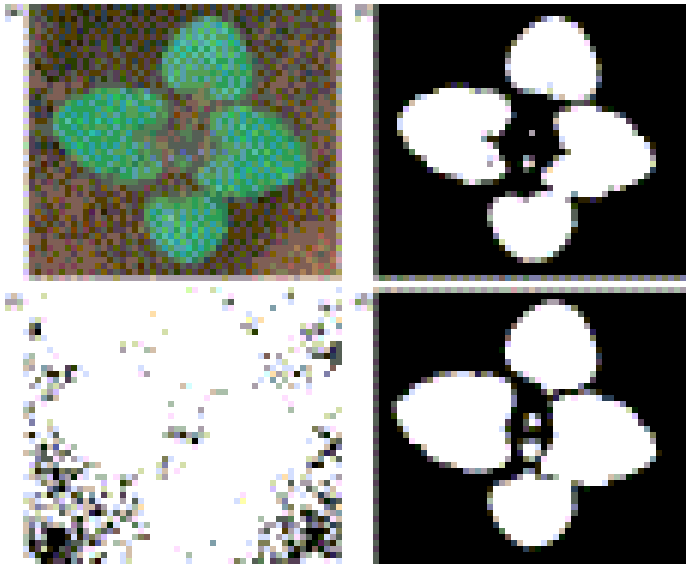

Liying Zheng, Jingtao Zhang, Qianyu Wang (2009)
Computers and Electronics in Agriculture 65(1): 93–98

Stereo vision

Biskup, B., Scharr, H., Schurr, U., & Rascher, U. (2007).
A stereo imaging system for measuring structural parameters of plant canopies.
Plant Cell and Environment, 30, 1299–1308

STEP 4: 3D reconstruction

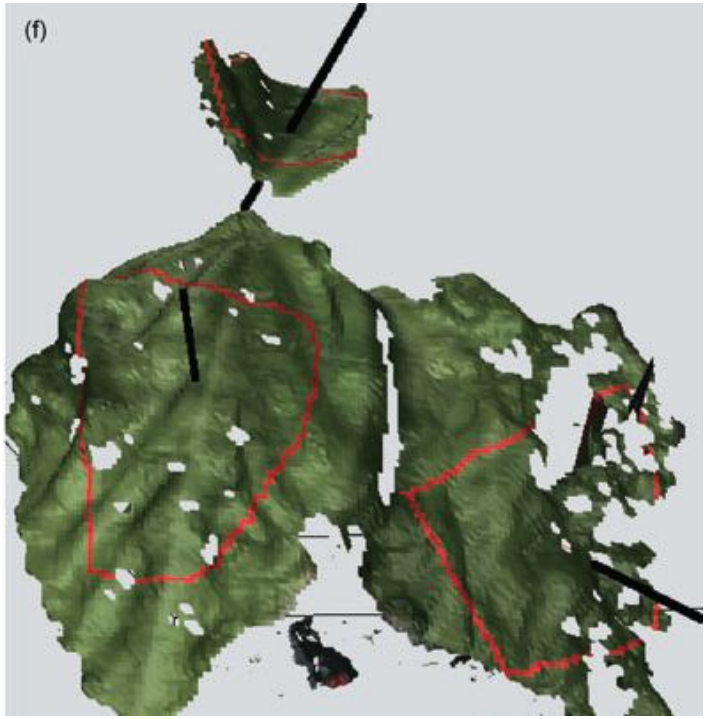

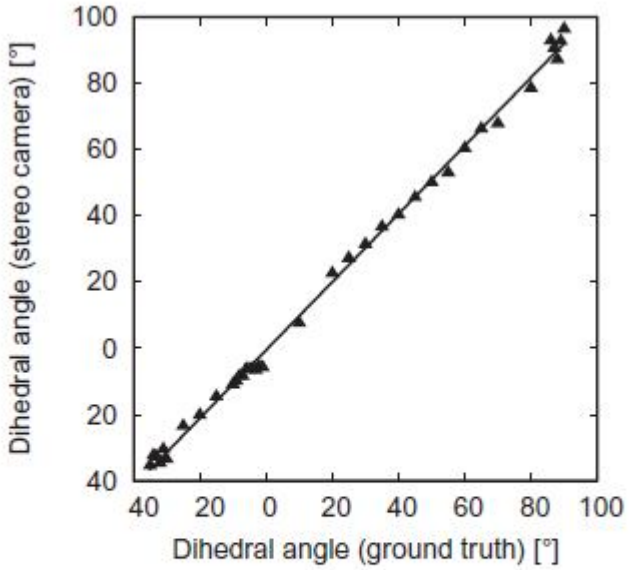

Figure 3. Accuracy of dihedral angle measurements. *X*-axis: reference angles obtained with water-level inclinometer. *Y*-axis: angles measured with stereo system. Line: linear regression ($y = 1.02x - 2.26$, $R^2 = 0.9937$). The stereo rig was directed 57° downward from the horizontal plane.

Stereo vision

Biskup, B., Scharr, H., Schurr, U., & Rascher, U. (2007).
A stereo imaging system for measuring structural parameters of plant canopies.
Plant Cell and Environment, 30, 1299–1308

STEP 4: 3D reconstruction

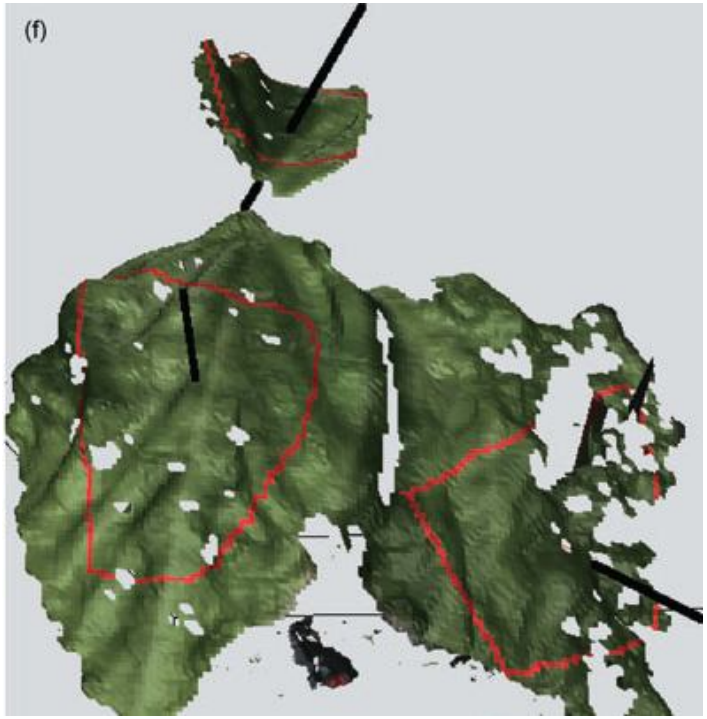

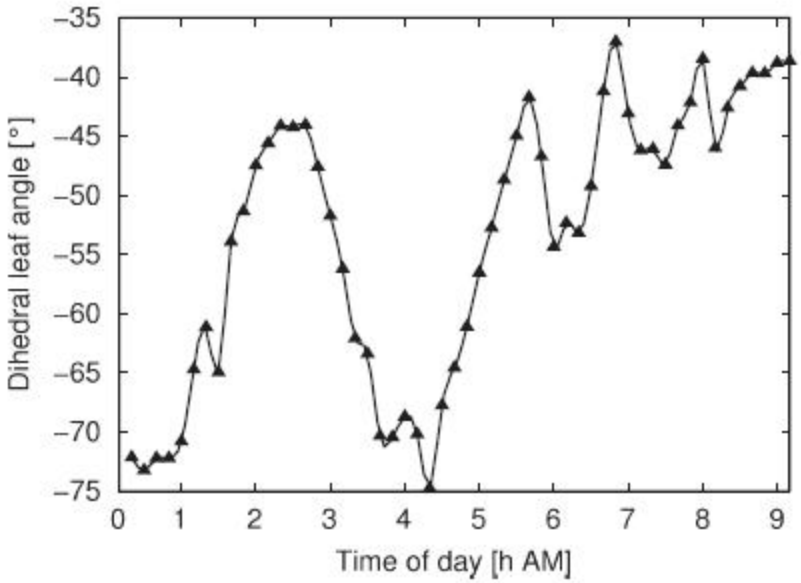

Figure 4. Leaf movement as quantified by stereo approach. Dihedral leaflet angle for one selected leaflet versus time. The measured leaflet angle results from a superimposition of longitudinal and lateral movement of the leaf under observation. Starting time: 0020 h; end time: 0920 h. Sunrise: 0554 h.

3D reconstruction

Passive methods– stereo imaging

– space carving

3D (cm x cm x cm)

Active methods – laser light detection and ranging, LIDAR

– structured light

Laser assisted line/point matching

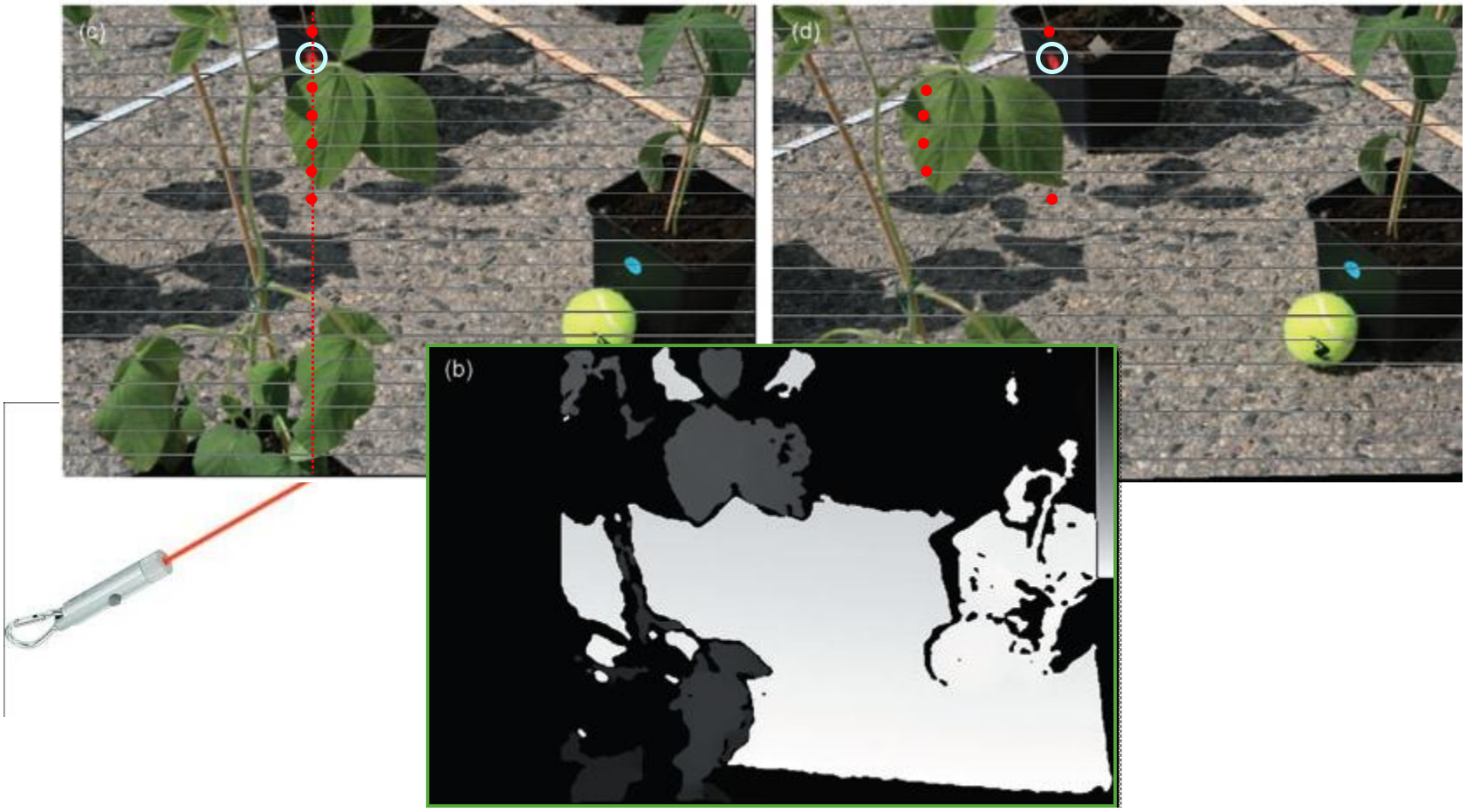

Projector line/point matching

Structured light 3D reconstruction

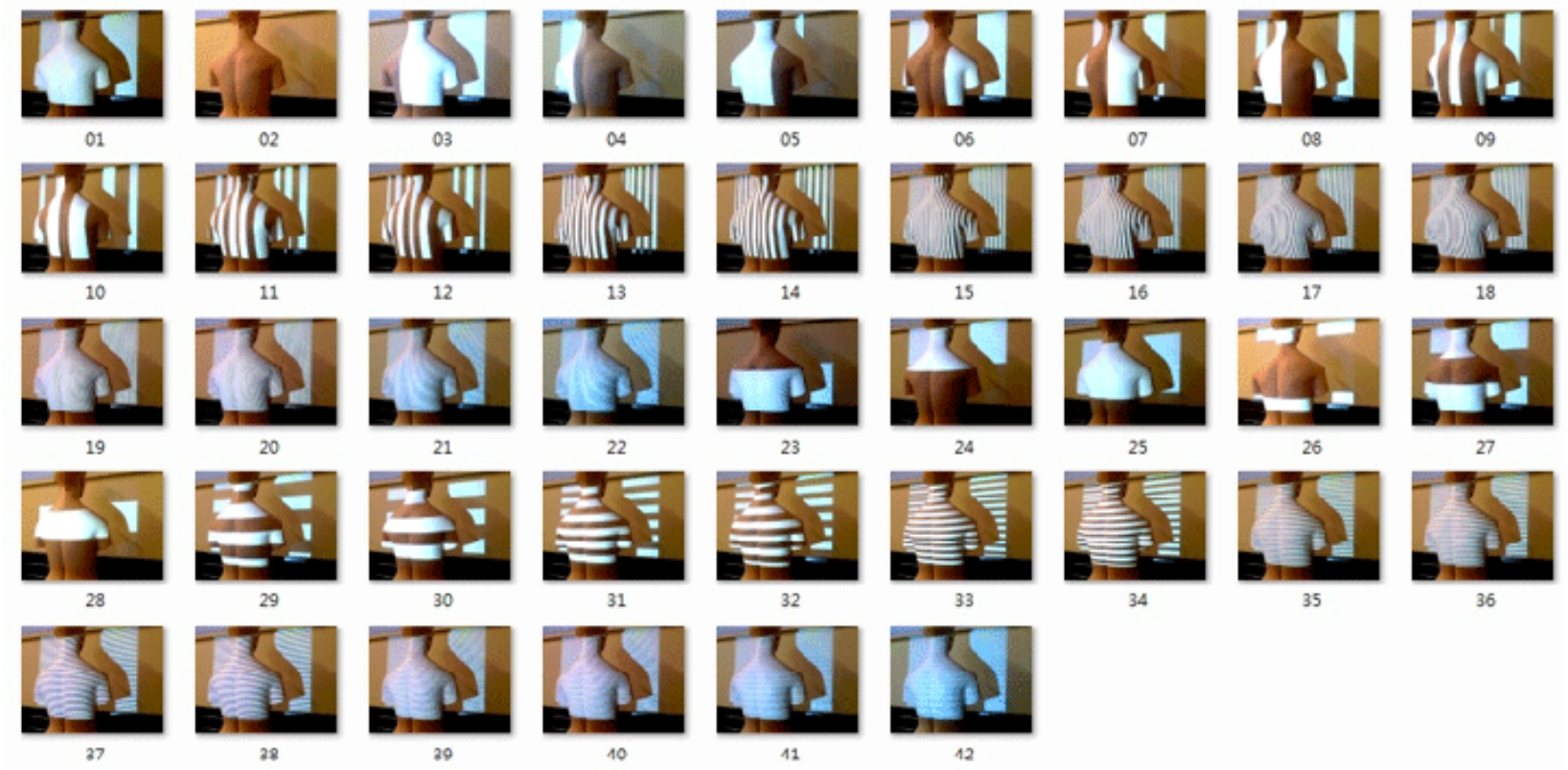

http://www.phys.canterbury.ac.nz/people/Chyou,%20Teyu.shtml

http://www.slideshare.net/dlanman/build-your-own-3d-scanner-course-notes

Structured light [3D + Chl-F]$_{(t)}$ imaging

Bellasio, C., Olejníčková, J., Tesař, R., Šebela, D. & Nedbal, L. (2012).
Computer Reconstruction of Plant Growth and Chlorophyll Fluorescence Emission in Three Spatial Dimensions. Sensors 2012, 12: 1052-1071

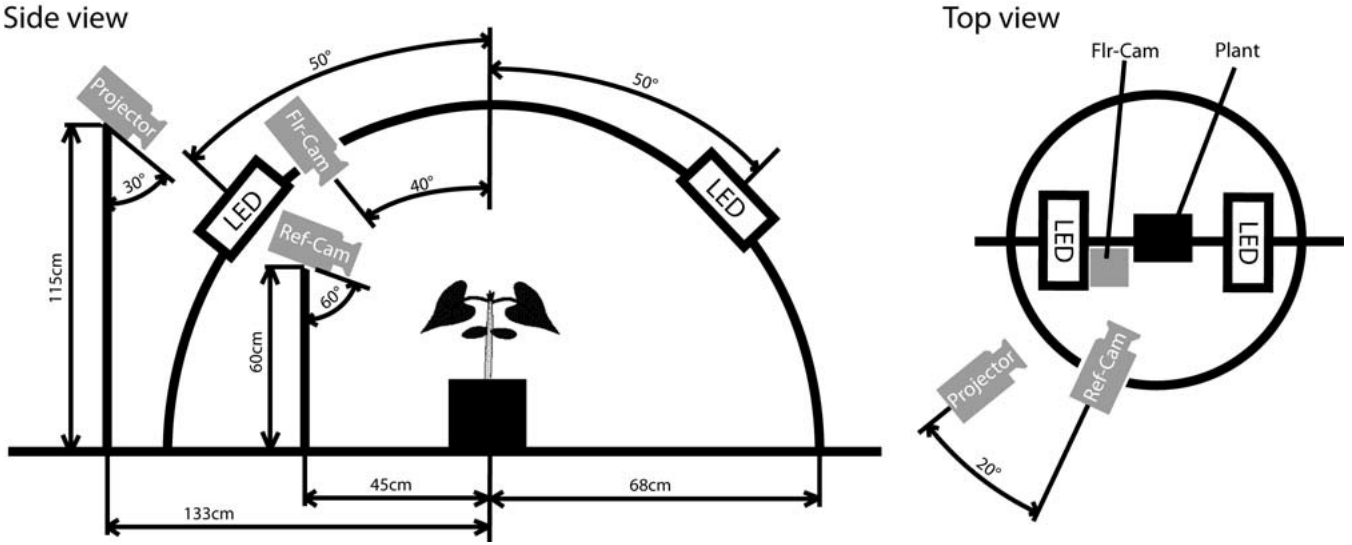

Structured light imaging

Bellasio, C., Olejníčková, J., Tesař, R., Šebela, D. & Nedbal, L. (2012).
Computer Reconstruction of Plant Growth and Chlorophyll Fluorescence Emission in Three Spatial Dimensions. Sensors 2012, 12: 1052-1071

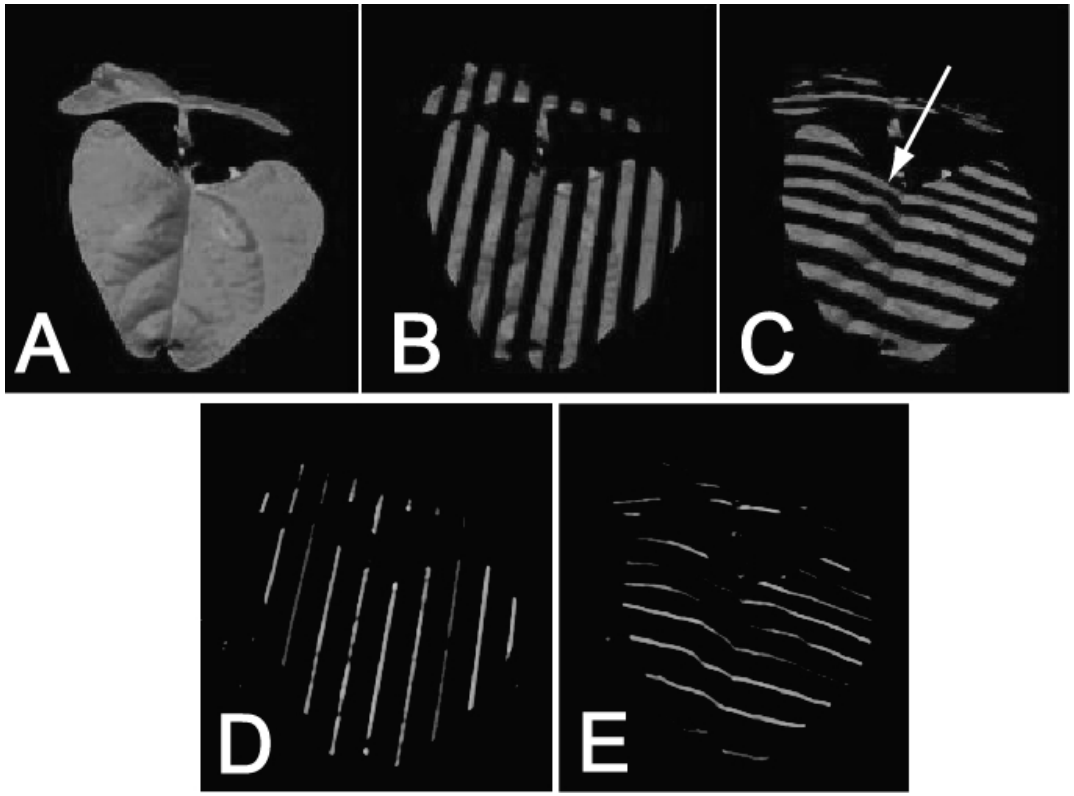

Structured light imaging – do it yourself

http://www.slideshare.net/dlanman/build-your-own-3d-scanner-course-notes

Structured light imaging – buy it and use SDK for your application

http://www.youtube.com/watch?v=zzb_RQWrt6I

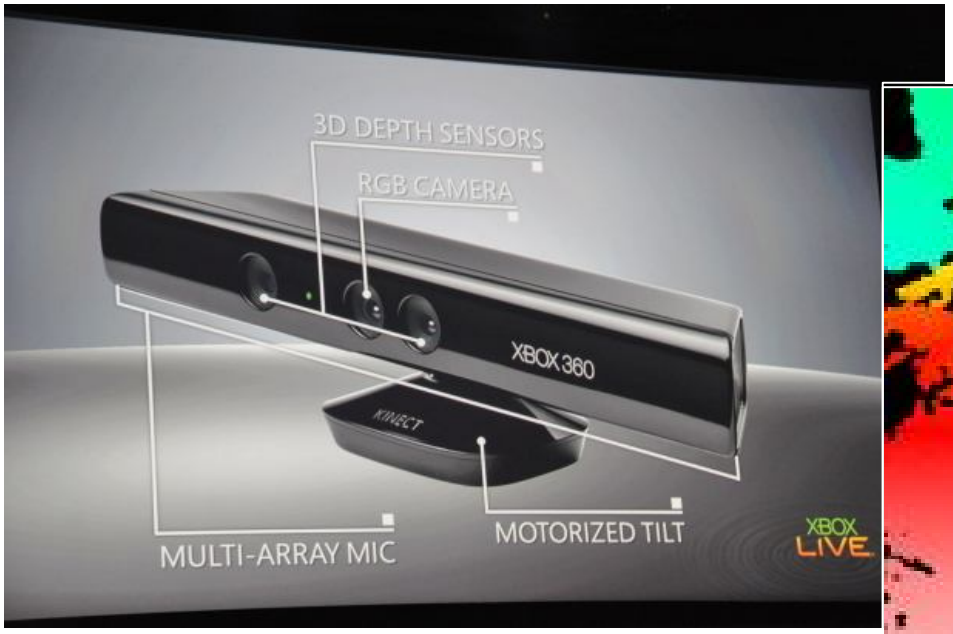

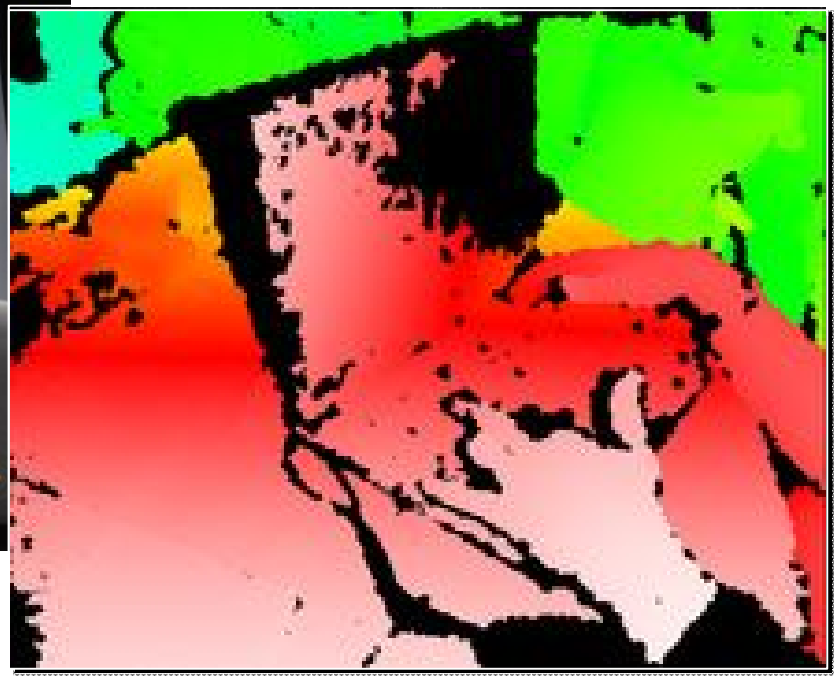

Structured light imaging – buy it and use SDK for your application

SCAN

3D reconstruction

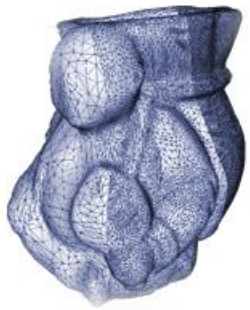

Add texture

1. Plant 3-D reconstruction
2. Adding Chl-fluorescence in time to 5-D
3. Statistical feature selection and combinatorial imaging

Structured light [3D + Chl-F]$_{(t)}$ imaging

Bellasio, C., Olejníčková, J., Tesař, R., Šebela, D. & Nedbal, L. (2012).
Computer Reconstruction of Plant Growth and Chlorophyll Fluorescence Emission in Three Spatial Dimensions. Sensors 2012, 12: 1052-1071

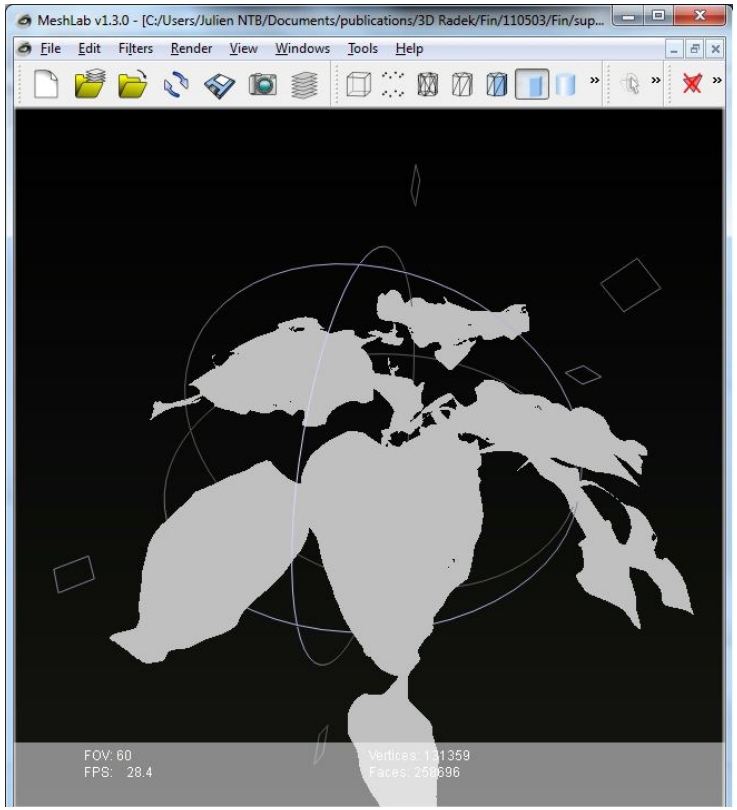

meshlab.sourceforge.net/

Figure 9. Distribution of Rfd100 parameter over water stressed pepper plants

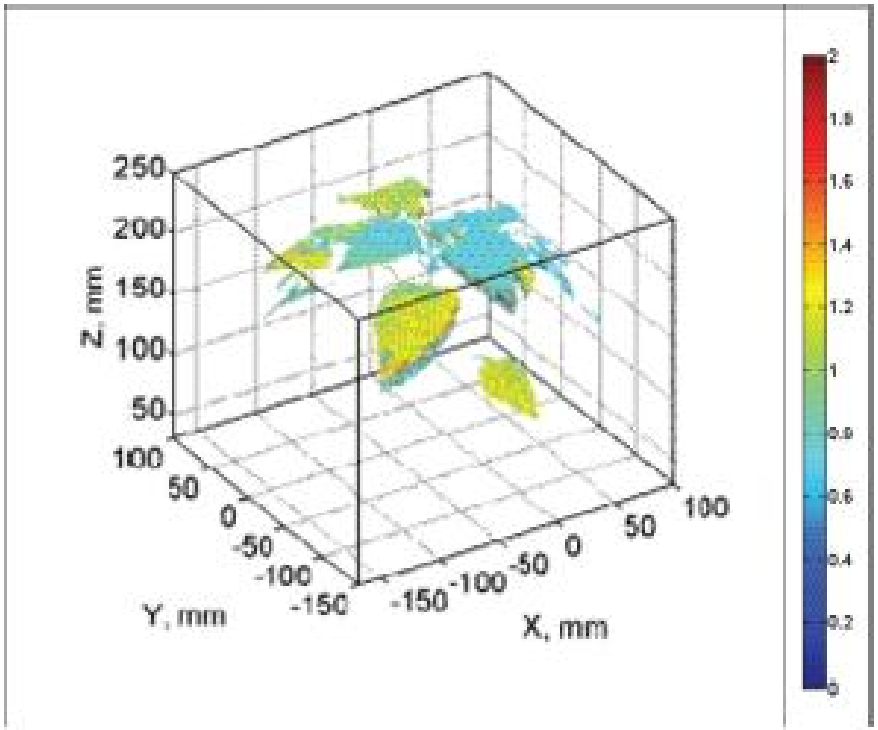

LIDAR (Light Detection and Ranging)

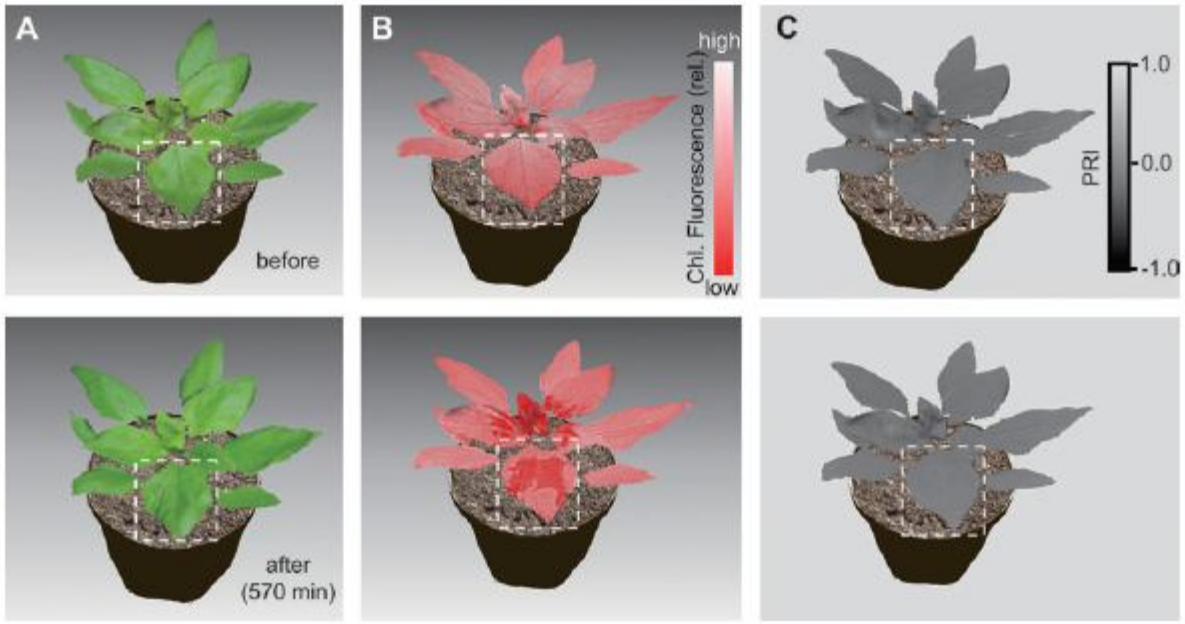

Fig. 12. Changes in 3D composite images of (A) the natural colour of a sunflower (*Helianthus annuus* L.) plant, (B) of chlorophyll (Chl.) *a* fluorescence intensity ('P' at the peak of the Kautsky effect), and (C) of the photochemical reflectance index (PRI) before (top row) and after (bottom row) treatment with glufosinate-ammonium (Basta) herbicide. The original 3D images were measured using an optical probe-based scanning lidar with 0.5 mm range accuracy. The composite images were obtained using a texture-mapping technique that mapped the natural colour, chlorophyll *a* fluorescence intensity, and PRI images to each 3D image. Broken lines show the part of the leaf to which the herbicide was applied. The upper images were measured ~180 min before the herbicide treatment and the lower ones were recorded ~570 min after the treatment. PPFD for fluorescence measurement (Omasa *et al.*, 1987) was 250 μmol m^{-2} s^{-1}. Temperature and relative humidity were 25 °C and 50%, respectively. Growth conditions were the same as those described in Fig. 10.

Kenji Omasa*, Fumiki Hosoi and Atsumi Konishi

Journal of Experimental Botany, Vol. 58, No. 4, pp. 881–898, 2007
Imaging Stress Responses in Plants Special Issue

Structured light [3D + Chl-F]$_{(t)}$ imaging

Bellasio, C., Olejníčková, J., Tesař, R., Šebela, D. & Nedbal, L. (2012).
Computer Reconstruction of Plant Growth and Chlorophyll Fluorescence Emission in Three Spatial Dimensions. Sensors 2012, 12: 1052-1071

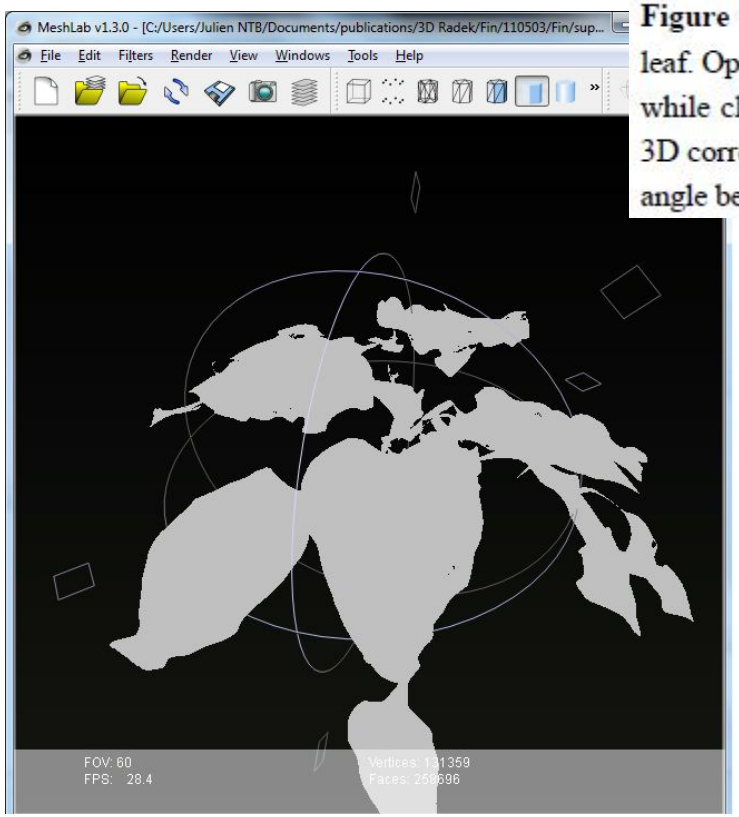

Figure 10. Distribution of steady state (Fs) chlorophyll fluorescence emission of a pepper leaf. Open symbols [○] show the distribution of fluorescence as recorded by FluorCam image while closed symbols represent the same values corrected for the leaf inclination [●]. The 3D corrected data were calculated by renormalizing the fluorescence signal by cosine of the angle between the normal to the leaf surface and the optical axes of the camera.

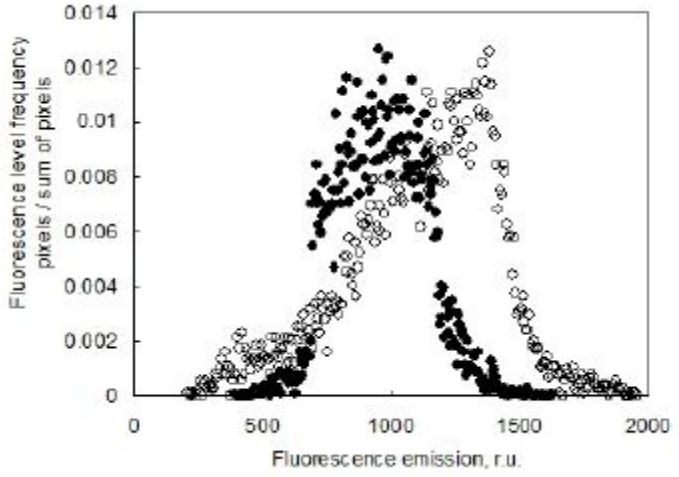

meshlab.sourceforge.net/

Chl-$F_{(t)}$ as a powerful reporter signal

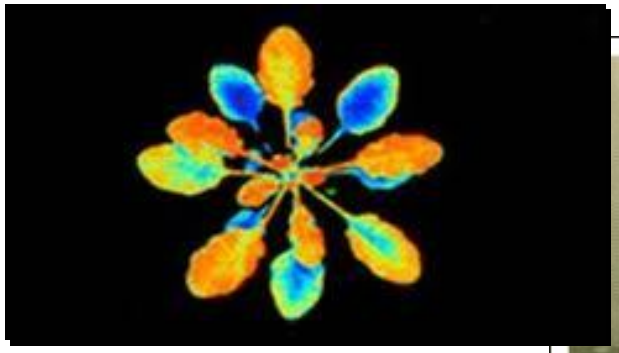

Current Opinion in Biotechnology

Chl-$F_{(t)}$ as a powerful reporter signal

Recent reviews:

- Harbinson J (2013) Improving the accuracy of chlorophyll fluorescence measurements. Plant, Cell and Environment, DOI: 10.1111/pce.12115
- Baker N.R. (2008), Chlorophyll fluorescence: a probe of photosynthesis *in vivo*. Annual Review of Plant Biology 59, 89-113

Recent advances:

- Earl H.J. & Ennahli S. (2004), Estimating photosynthetic electron transport via chlorophyll fluorometry without Photosystem II light saturation. Photosynthesis Research 82, 177-186
- Loriaux S, Avenson T, Welles J, McDermitt D, Eckles R, Riensche B, and Genty, B. (2013) Closing in on maximum yield of chlorophyll fluorescence using a single multiphase flash of subsaturating intensity. Plant, Cell and Environment, DOI: 10.1111/pce.12115

Photosynthesis

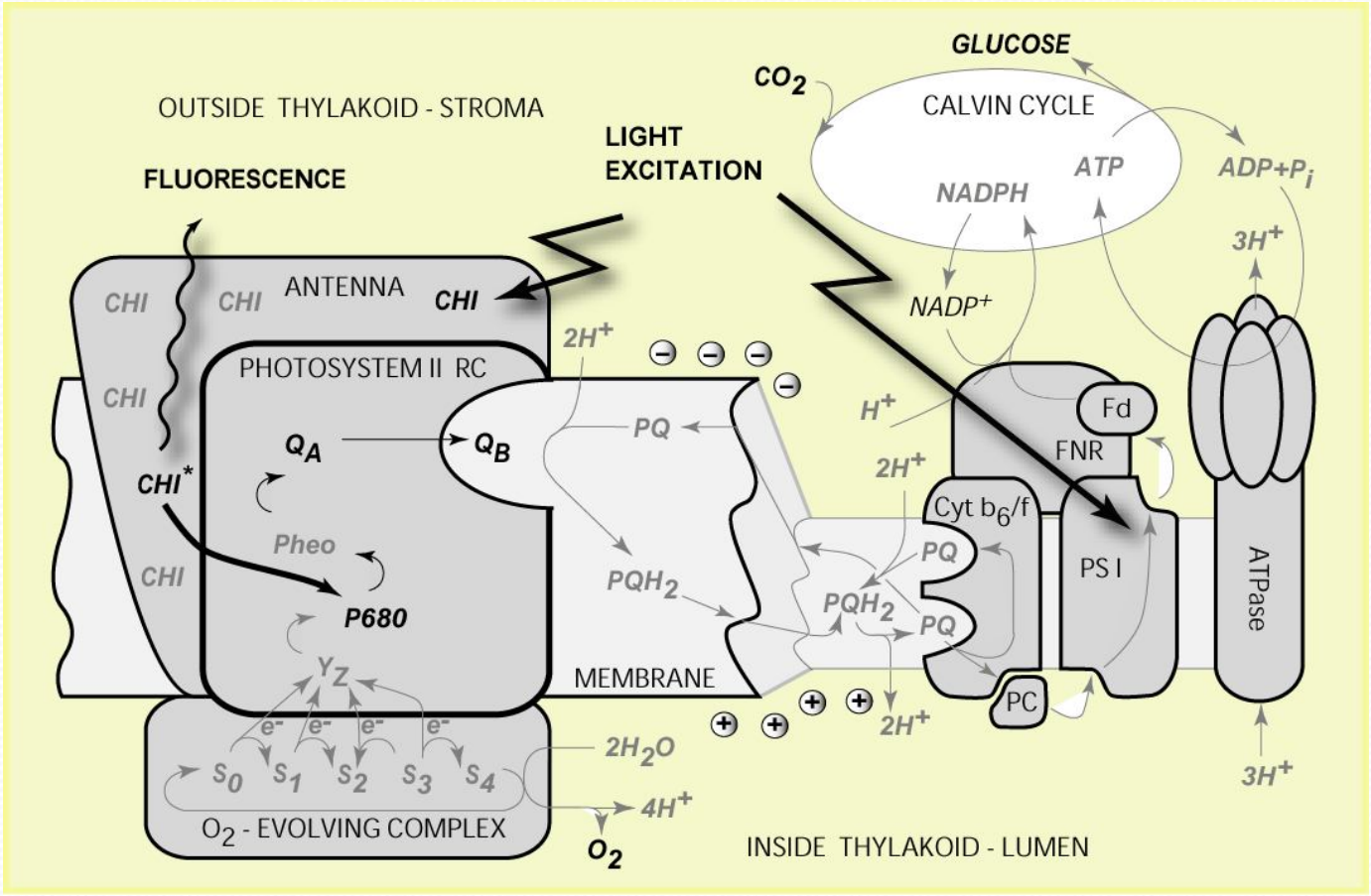

Chlorophyll fluorescence emission & PSII activity

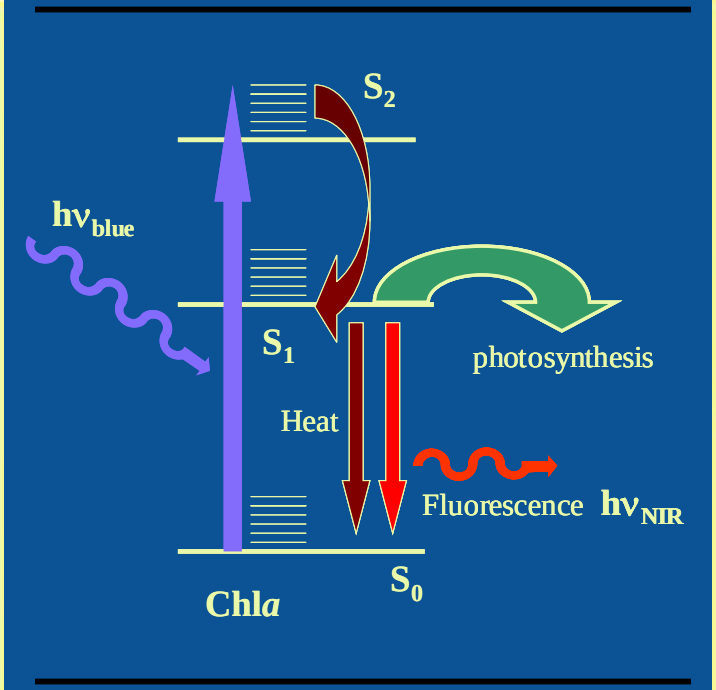

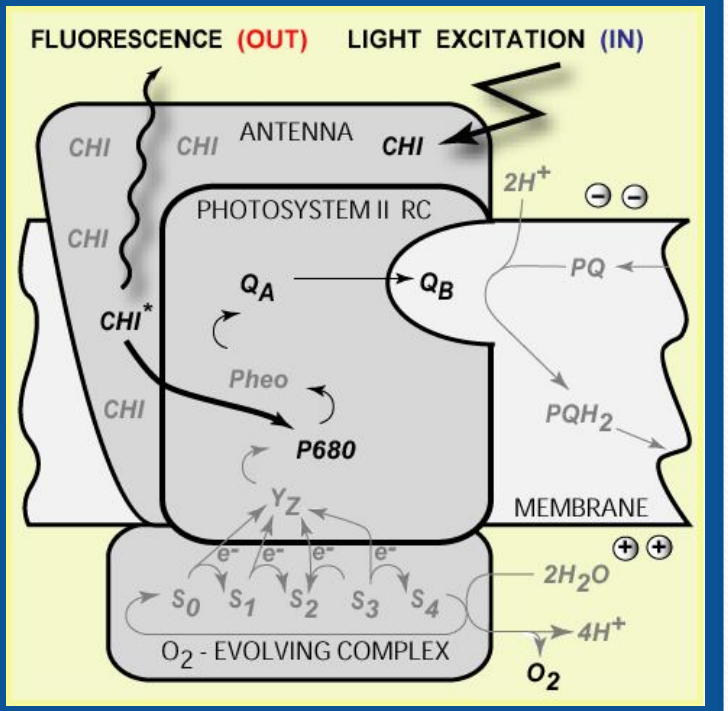

Chlorophyll fluorescence emission & PSII activity in a flash

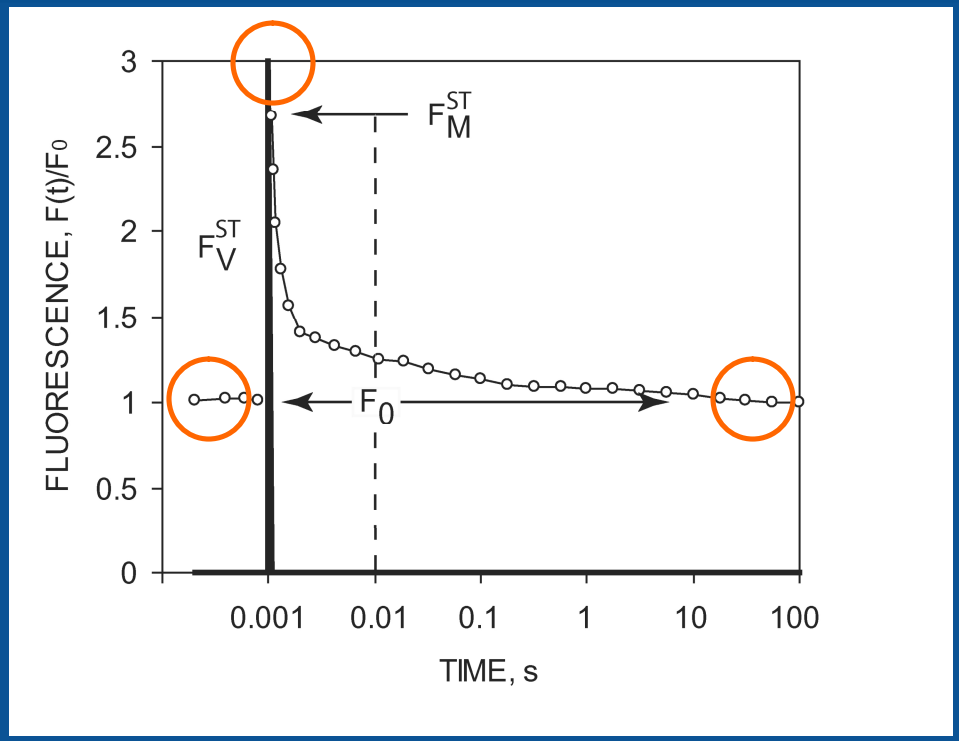

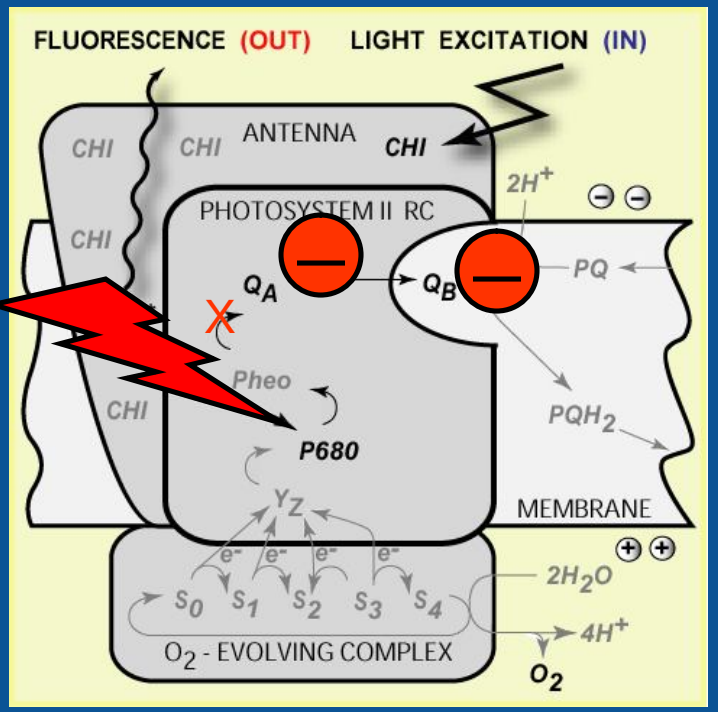

Parameter	Definition	Physiological relevance
F, F'	Fluorescence emission from dark- or light-adapted leaf, respectively.	Provides little information on photosynthetic performance because these parameters are influenced by many factors. F' is sometimes referred to as F_s' when at steady state
F_o, F_o'	Minimal fluorescence from dark- and light-adapted leaf, respectively	Level of fluorescence when Q_A is maximally oxidized (PSII centers open)
F_m, F_m'	Maximal fluorescence from dark- and light-adapted leaf, respectively	Level of fluorescence when Q_A is maximally reduced (PSII centers closed)
F_v, F_v'	Variable fluorescence from dark- and light-adapted leaves, respectively	Demonstrates the ability of PSII to perform photochemistry (Q_A reduction)
F_q'	Difference in fluorescence between F_m' and F'	Photochemical quenching of fluorescence by open PSII centers.
F_v/F_m	Maximum quantum efficiency of PSII photochemistry	Maximum efficiency at which light absorbed by PSII is used for reduction of Q_A.
F_q'/F_m'	PSII operating efficiency	Estimates the efficiency at which light absorbed by PSII is used for Q_A reduction. At a given photosynthetically active photon flux density (PPFD) this parameter provides an estimate of the quantum yield of linear electron flux through PSII. This parameter has previously been termed $\Delta F/F_m'$ and ϕ_{PSII} in the literature.
F_v'/F_m'	PSII maximum efficiency	Provides an estimate of the maximum efficiency of PSII photochemistry at a given PPFD, which is the PSII operating efficiency if all the PSII centers were 'open' (Q_A oxidized).
F_q'/F_v'	PSII efficiency factor	Relates the PSII maximum efficiency to the PSII operating efficiency. Nonlinearly related to the proportion of PSII centers that are 'open' (Q_A oxidized). Mathematically identical to the coefficient of photochemical quenching, q_P.
NPQ	Nonphotochemical quenching	Estimates the nonphotochemical quenching from F_m to F_m'. Monitors the apparent rate constant for heat loss from PSII. Calculated from $(F_m/F_m') - 1$.
q_E	Energy-dependent quenching	Associated with light-induced proton transport into the thylakoid lumen. Regulates the rate of excitation of PSII reaction centers.
q_I	Photoinhibitory quenching	Results from photoinhibition of PSII photochemistry.
q_L	Fraction of PSII centers that are 'open'	Estimates the fraction of 'open' PSII centers (with Q_A oxidized) on the basis of a lake model for the PSII photosynthetic apparatus. Given by $(F_q'/F_v')(F_o'/F')$
q_T	Quenching associated with a state transition	Results from phosphorylation of light-harvesting complexes associated with PSII
ϕ_F	Quantum yield of fluorescence	Number of fluorescent events for each photon absorbed

Baker N.R. (2008), Chlorophyll fluorescence: a probe of photosynthesis *in vivo*. Ann. Rev Plant Biol 59: 89-113

Two roles of light in Chl-fluorescence experiments

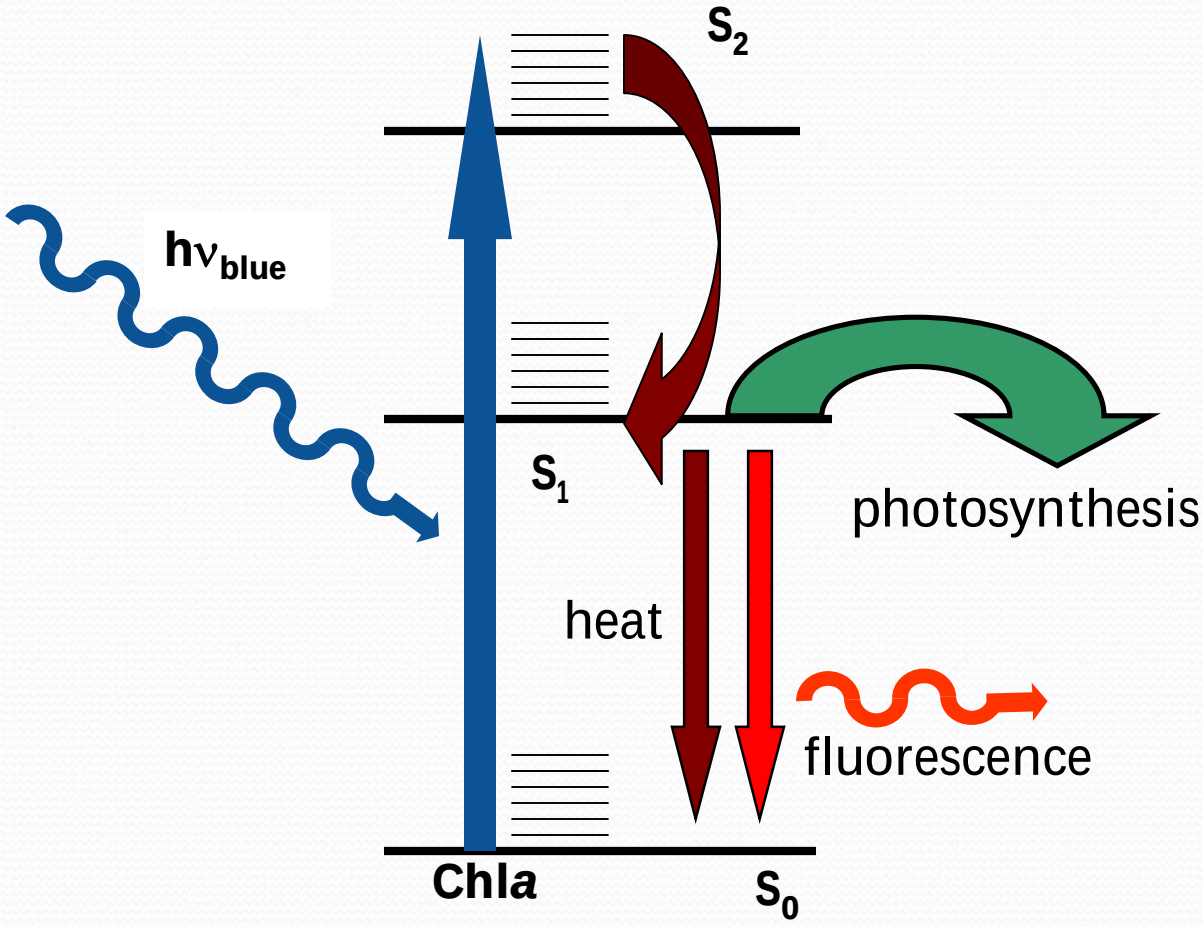

Measuring light ("dark")

$$\Phi_F = \Phi_{Fo} = \frac{k_F}{k_F + k_N + k_P}$$

Aim: Excite the fluorescence-emitting pigment molecules without changing the experimental photo-chemically active object. Fluorescence should be distinguishable from background of the same color.

Achieved by MEASURING light:
Typically 10-30μs long flashes repeated with a low frequency that

Schreiber U. 2004. Pulse-Amplitude-Modulation (PAM) fluorometry and saturation pulse method: an overview. *Chlorophyll a Fluorescence: A Signature of Photosynthesis*, ed. GC Papageorgiou, Govindjee, pp. 279–319. Dordrecht, The Netherlands: Springer

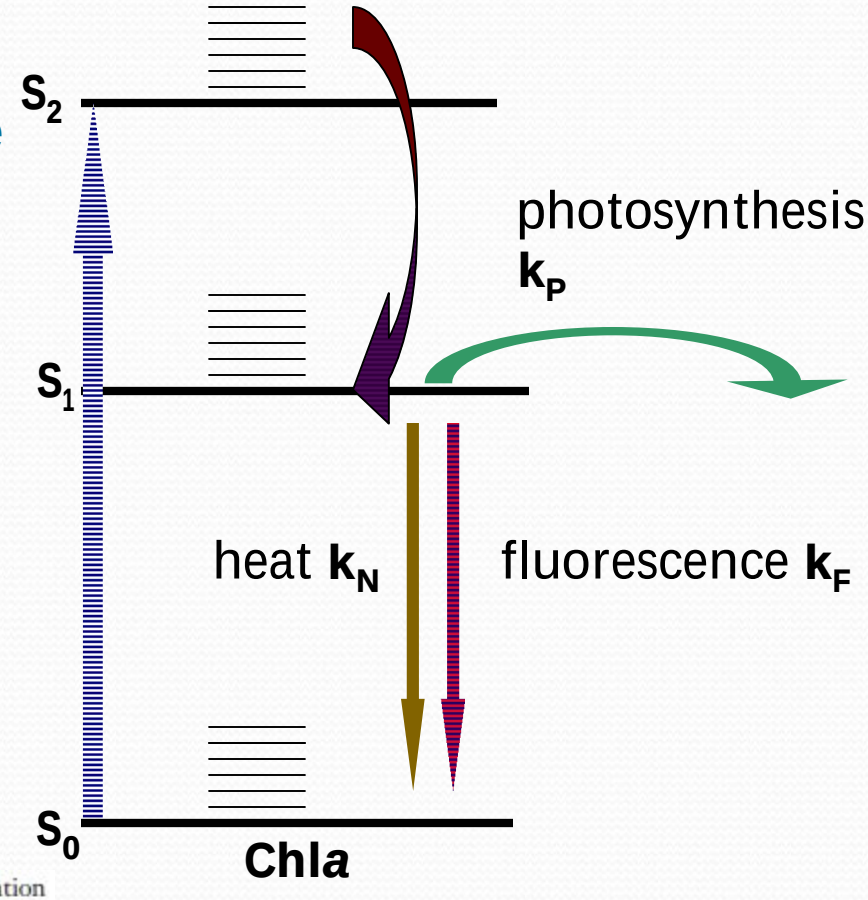

Schreiber, U., Schliwa, U., and Bilger, W. 1986, Photosynth. Res., 10, 51.

Saturating pulse

$$\Phi_F = \Phi_{Fm} = \frac{k_F}{k_F + k_N}$$

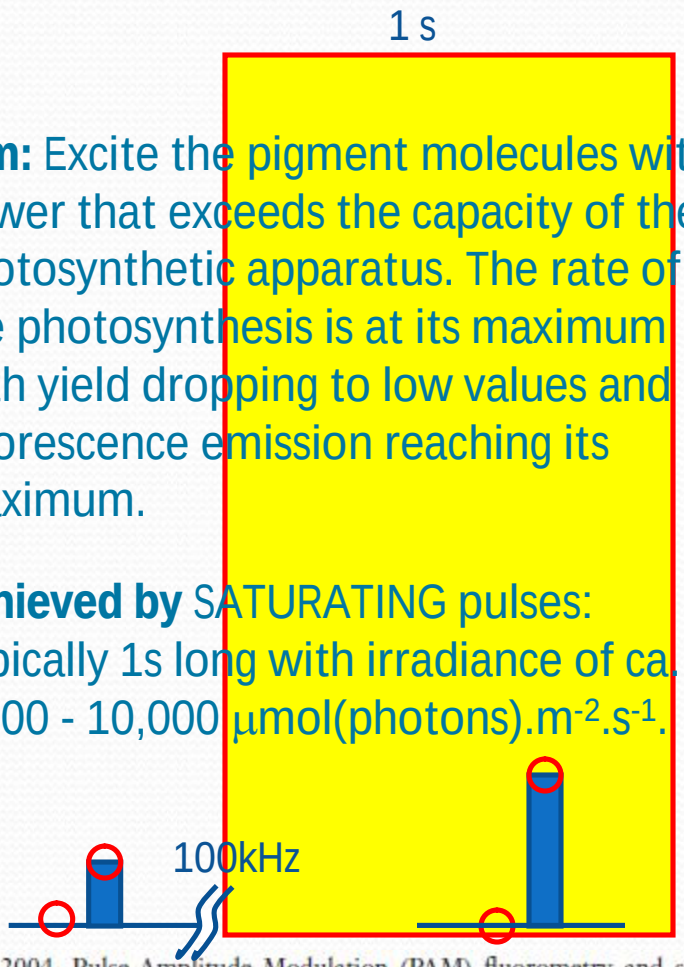

Aim: Excite the pigment molecules with a power that exceeds the capacity of the photosynthetic apparatus. The rate of the photosynthesis is at its maximum with yield dropping to low values and fluorescence emission reaching its maximum.

Achieved by SATURATING pulses: Typically 1s long with irradiance of ca. 2,000 - 10,000 μmol(photons).$m^{-2}.s^{-1}$.

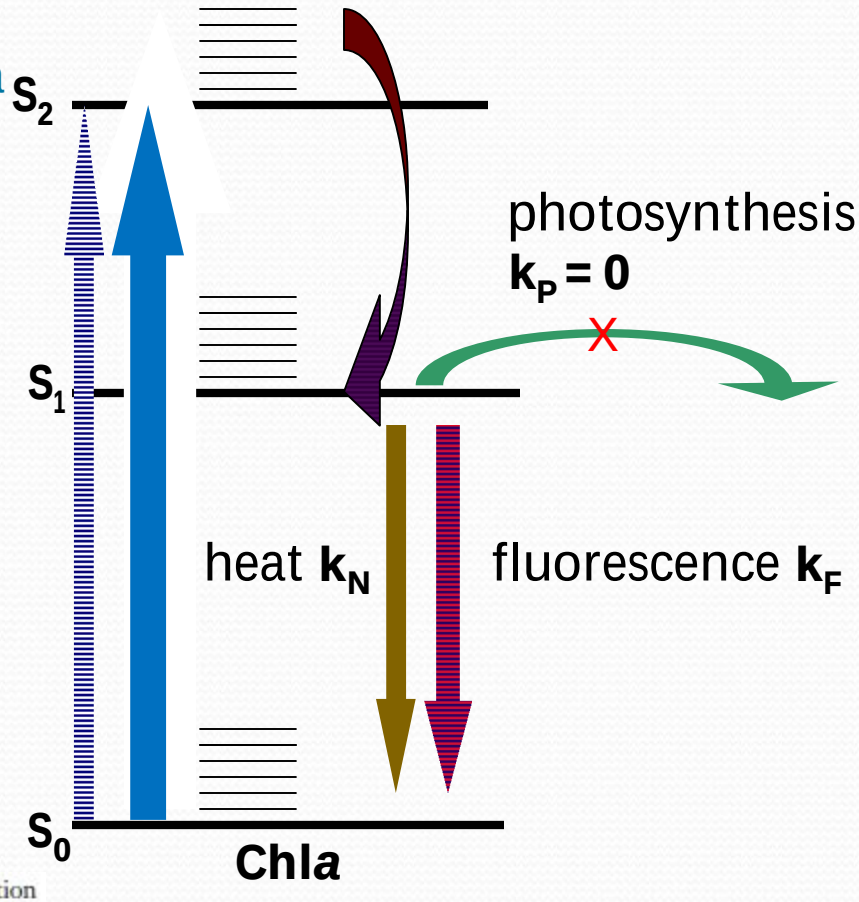

Schreiber U. 2004. Pulse-Amplitude-Modulation (PAM) fluorometry and saturation pulse method: an overview. *Chlorophyll a Fluorescence: A Signature of Photosynthesis*, ed. GC Papageorgiou, Govindjee, pp. 279–319. Dordrecht, The Netherlands: Springer

Schreiber, U., Schliwa, U., and Bilger, W. 1986, Photosynth. Res., 10, 51.

A bit of algebra ...

$$F_m = (I \cdot N \cdot \sigma) \cdot \Phi_{Fm} = (I \cdot N \cdot \sigma) \frac{k_F}{k_F + k_N}$$

$$F_0 = (I \cdot N \cdot \sigma) \frac{k_F}{k_F + k_N + k_P}$$

$$\frac{F_m - F_0}{F_m} = \frac{F_m - F_0}{F_m} = 1 - \frac{\frac{k_F}{k_F + k_N + k_P}}{\frac{k_F}{k_F + k_N}} = \frac{(k_F + k_N + k_P) - (k_F + k_N)}{k_F + k_N + k_P}$$

$$\frac{F_v}{F_m} = \frac{k_P}{k_F + k_N + k_P} = \Phi_{Pmax}$$

Genty B, Briantais J-M, Baker NR. 1989. The relationship between the quantum yield of photosynthetic electron transport and quenching of chlorophyll fluorescence. *Biochim. Biophys. Acta* 990:87–92

Dark-adapted **Actinic light** **Dark**

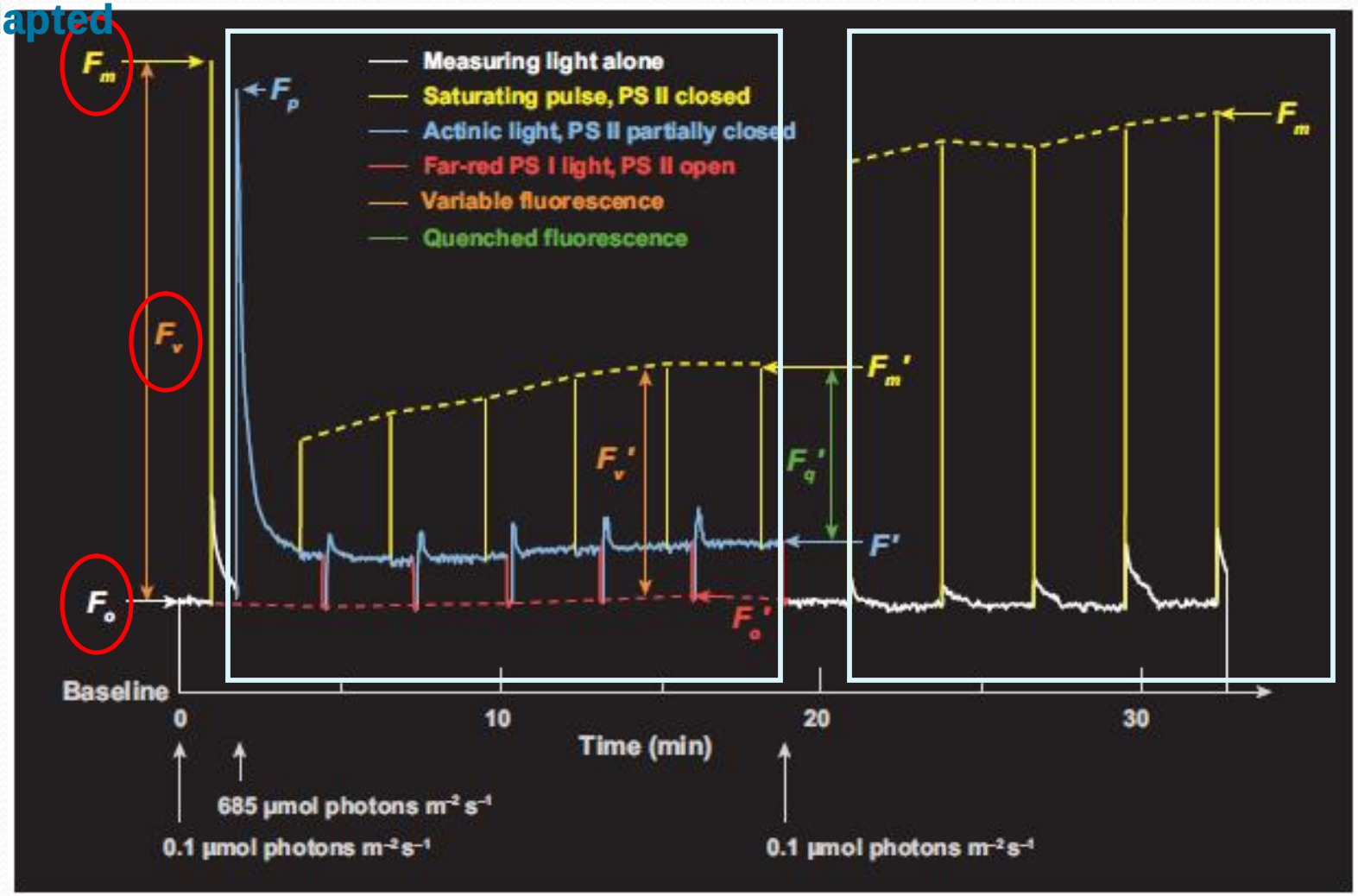

Baker N.R. (2008), Chlorophyll fluorescence: a probe of photosynthesis *in vivo*. Ann. Rev Plant Biol 59: 89-113

Parameter	Definition	Physiological relevance
F, F'	Fluorescence emission from dark- or light-adapted leaf, respectively.	Provides little information on photosynthetic performance because these parameters are influenced by many factors. F' is sometimes referred to as F_s' when at steady state
F_o, F_o'	Minimal fluorescence from dark- and light-adapted leaf, respectively	Level of fluorescence when Q_A is maximally oxidized (PSII centers open)
F_m, F_m'	Maximal fluorescence from dark- and light-adapted leaf, respectively	Level of fluorescence when Q_A is maximally reduced (PSII centers closed)
F_v, F_v'	Variable fluorescence from dark- and light-adapted leaves, respectively	Demonstrates the ability of PSII to perform photochemistry (Q_A reduction)
F_q'	Difference in fluorescence between F_m' and F'	Photochemical quenching of fluorescence by open PSII centers.
F_v/F_m	Maximum quantum efficiency of PSII photochemistry	Maximum efficiency at which light absorbed by PSII is used for reduction of Q_A.
F_q'/F_m'	PSII operating efficiency	Estimates the efficiency at which light absorbed by PSII is used for Q_A reduction. At a given photosynthetically active photon flux density (PPFD) this parameter provides an estimate of the quantum yield o parameter has p literature.
F_v'/F_m'	PSII maximum efficiency	Provides an esti photochemistry efficiency if all t
F_q'/F_v'	PSII efficiency factor	Relates the PSII r efficiency. Nonli that are 'open' (coefficient of ph
NPQ	Nonphotochemical quenching	Estimates the no Monitors the ap Calculated from
q_E	Energy-dependent quenching	Associated with li lumen. Regulate
q_I	Photoinhibitory quenching	Results from pho
q_L	Fraction of PSII centers that are 'open'	Estimates the frac the basis of a lak Given by (F_q'/F_v
q_T	Quenching associated with a state transition	Results from phos associated with I
ϕ_F	Quantum yield of fluorescence	Number of fluorescent events for each photon absorbed

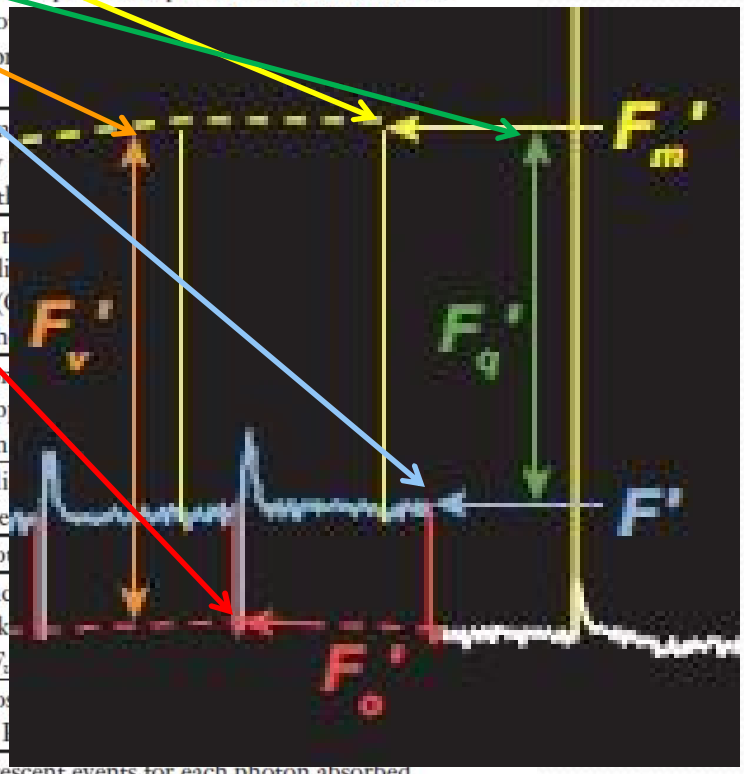

Baker N.R. (2008), Chlorophyll fluorescence: a probe of photosynthesis *in vivo*. Ann. Rev Plant Biol 59: 89-113

Parameter	Definition	Physiological relevance
F, F'	Fluorescence emission from dark- or light-adapted leaf, respectively.	Provides little information on photosynthetic performance because these parameters are influenced by many factors. F' is sometimes referred to as F_s' when at steady state
F_o, F_o'	Minimal fluorescence from dark- and light-adapted leaf, respectively	Level of fluorescence when Q_A is maximally oxidized (PSII centers open)
F_m, F_m'	Maximal fluorescence from dark- and light-adapted leaf, respectively	Level of fluorescence when Q_A is maximally reduced (PSII centers closed)
F_v, F_v'	Variable fluorescence from dark- and light-adapted leaves, respectively	Demonstrates the ability of PSII to perform photochemistry (Q_A reduction)
F_q'	Difference in fluorescence between F_m' and F'	Photochemical quenching of fluorescence by open PSII centers.
F_v/F_m	Maximum quantum efficiency of PSII photochemistry	Maximum efficiency at which light absorbed by PSII is used for reduction of Q_A.
F_q'/F_m'	PSII operating efficiency	Estimates the efficiency at which light absorbed by PSII is used for Q_A reduction. At a given photosynthetically active photon flux density (PPFD) this parameter provides an estimate of the quantum yield of linear electron flux through PSII. This parameter has previously been termed $\Delta F/F_m'$ and ϕ_{PSII} in the literature.
F_v'/F_m'	PSII maximum efficiency	Provides an estimate photochemistry at a efficiency if all the
F_q'/F_v'	PSII efficiency factor	Relates the PSII ma efficiency. Nonlinea that are 'open' (Q_A coefficient of photo
NPQ	Nonphotochemical quenching	Estimates the nonph Monitors the appar Calculated from ($F_$
q_E	Energy-dependent quenching	Associated with light lumen. Regulates th
q_I	Photoinhibitory quenching	Results from photoi
q_L	Fraction of PSII centers that are 'open'	Estimates the fractio the basis of a lake m Given by (F_q'/F_v')(
q_T	Quenching associated with a state transition	Results from phosph associated with PSI
ϕ_F	Quantum yield of fluorescence	Number of fluoresce

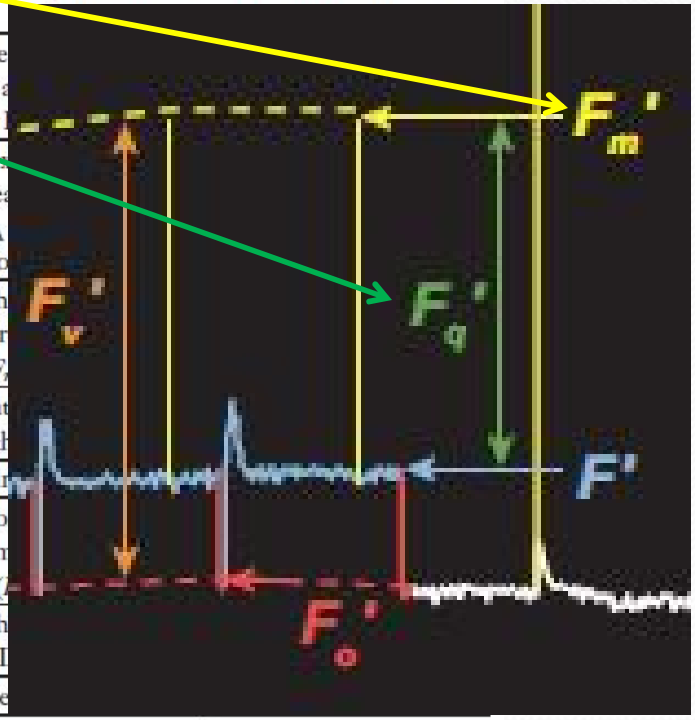

Baker N.R. (2008), Chlorophyll fluorescence: a probe of photosynthesis *in vivo*. Ann. Rev Plant Biol 59: 89-113

Parameter	Definition	
F, F'	Fluorescence emission from dark- or light-adapted leaf, respectively.	Provides little inf because these pa sometimes refer
F_o, F_o'	Minimal fluorescence from dark- and light-adapted leaf, respectively	Level of fluoresce open)
F_m, F_m'	Maximal fluorescence from dark- and light-adapted leaf, respectively	Level of fluoresce closed)
F_v, F_v'	Variable fluorescence from dark- and light-adapted leaves, respectively	Demonstrates the (Q_A reduction)
F_q'	Difference in fluorescence between F_m' and F'	Photochemical qu
F_v/F_m	Maximum quantum efficiency of PSII photochemistry	Maximum efficien reduction of Q_A
F_q'/F_m'	PSII operating efficiency	Estimates the effi Q_A reduction. A density (PPFD) quantum yield o parameter has p literature.
F_v'/F_m'	PSII maximum efficiency	Provides an estimate of the maximum efficiency of PSII photochemistry at a given PPFD, which is the PSII operating efficiency if all the PSII centers were 'open' (Q_A oxidized).
F_q'/F_v'	PSII efficiency factor	Relates the PSII maximum efficiency to the PSII operating efficiency. Nonlinearly related to the proportion of PSII centers that are 'open' (Q_A oxidized). Mathematically identical to the coefficient of photochemical quenching, q_P.
NPQ	Nonphotochemical quenching	Estimates the nonphotochemical quenching from F_m to F_m'. Monitors the apparent rate constant for heat loss from PSII. Calculated from $(F_m/F_m') - 1$.
q_E	Energy-dependent quenching	Associated with light-induced proton transport into the thylakoid lumen. Regulates the rate of excitation of PSII reaction centers.
q_I	Photoinhibitory quenching	Results from photoinhibition of PSII photochemistry.
q_L	Fraction of PSII centers that are 'open'	Estimates the fraction of 'open' PSII centers (with Q_A oxidized) on the basis of a lake model for the PSII photosynthetic apparatus. Given by $(F_q'/F_v')(F_o'/F')$
q_T	Quenching associated with a state transition	Results from phosphorylation of light-harvesting complexes associated with PSII
ϕ_F	Quantum yield of fluorescence	Number of fluorescent events for each photon absorbed

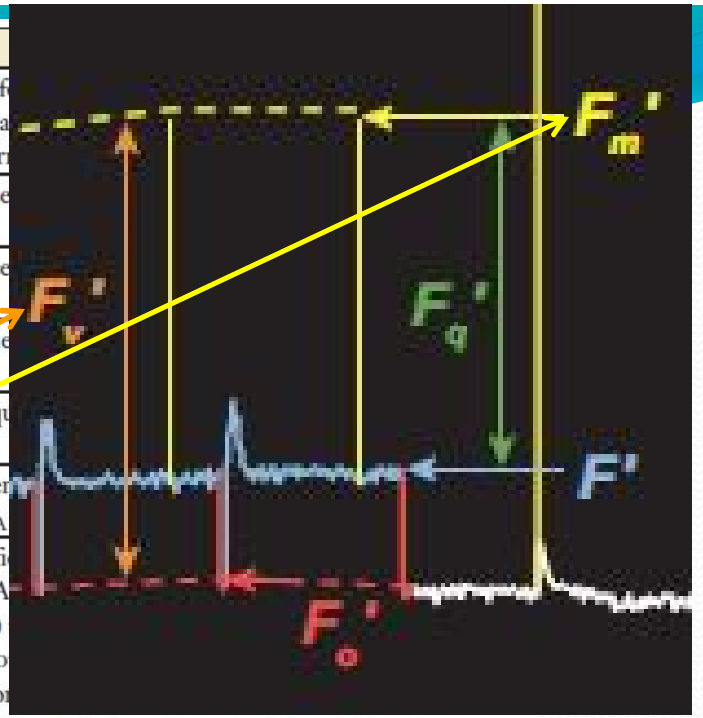

Baker N.R. (2008), Chlorophyll fluorescence: a probe of photosynthesis *in vivo*. Ann. Rev Plant Biol 59: 89-113

Parameter	Definition	
F, F'	Fluorescence emission from dark- or light-adapted leaf, respectively.	Provides little inf because these pa sometimes refer
F_o, F_o'	Minimal fluorescence from dark- and light-adapted leaf, respectively	Level of fluoresce open)
F_m, F_m'	Maximal fluorescence from dark- and light-adapted leaf, respectively	Level of fluoresce closed)
F_v, F_v'	Variable fluorescence from dark- and light-adapted leaves, respectively	Demonstrates the (Q_A reduction)
F_q'	Difference in fluorescence between F_m' and F'	Photochemical qu
F_v/F_m	Maximum quantum efficiency of PSII photochemistry	Maximum efficie reduction of Q_A
F_q'/F_m'	PSII operating efficiency	Estimates the effi Q_A reduction. A density (PPFD) quantum yield o parameter has p literature.
F_v'/F_m'	PSII maximum efficiency	Provides an estimate of the maximum efficiency of PSII photochemistry at a given PPFD, which is the PSII operating efficiency if all the PSII centers were 'open' (Q_A oxidized).
F_q'/F_v'	PSII efficiency factor	Relates the PSII maximum efficiency to the PSII operating efficiency. Nonlinearly related to the proportion of PSII centers that are 'open' (Q_A oxidized). Mathematically identical to the coefficient of photochemical quenching, q_P.
NPQ	Nonphotochemical quenching	Estimates the nonphotochemical quenching from F_m to F_m'. Monitors the apparent rate constant for heat loss from PSII. Calculated from $(F_m/F_m') - 1$.
q_E	Energy-dependent quenching	Associated with light-induced proton transport into the thylakoid lumen. Regulates the rate of excitation of PSII reaction centers.
q_I	Photoinhibitory quenching	Results from photoinhibition of PSII photochemistry.
q_L	Fraction of PSII centers that are 'open'	Estimates the fraction of 'open' PSII centers (with Q_A oxidized) on the basis of a lake model for the PSII photosynthetic apparatus. Given by $(F_q'/F_v')(F_o'/F')$
q_T	Quenching associated with a state transition	Results from phosphorylation of light-harvesting complexes associated with PSII
ϕ_F	Quantum yield of fluorescence	Number of fluorescent events for each photon absorbed

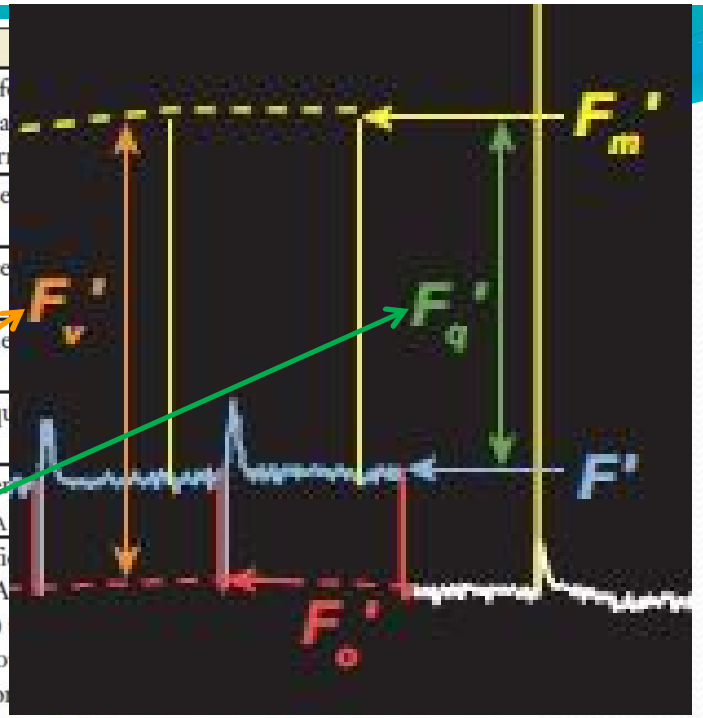

Baker N.R. (2008), Chlorophyll fluorescence: a probe of photosynthesis *in vivo*. Ann. Rev Plant Biol 59: 89-113

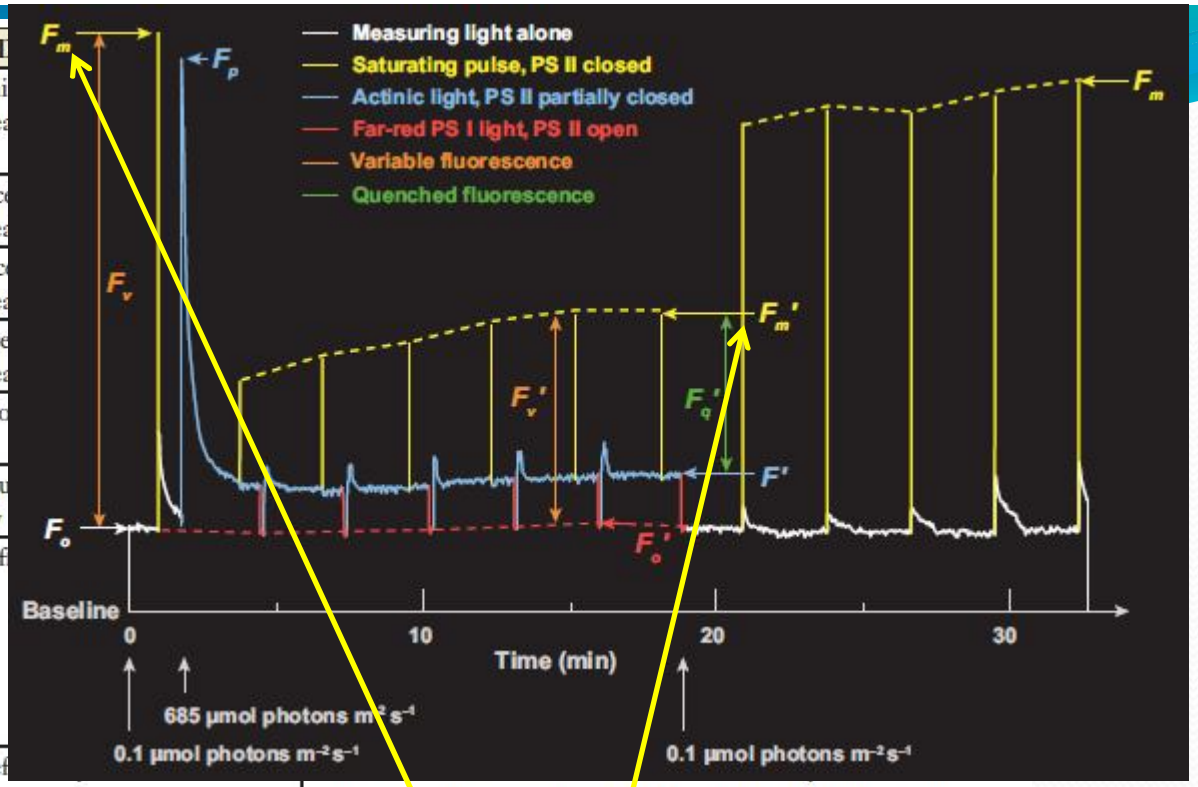

Parameter		
F, F'	Fluorescence emi light-adapted le	
F_o, F_o'	Minimal fluoresc light-adapted le	
F_m, F_m'	Maximal fluoresc light-adapted le	
F_v, F_v'	Variable fluoresc light-adapted le	
F_q'	Difference in fluo and F'	
F_v/F_m	Maximum quantu photochemistry	
F_q'/F_m'	PSII operating ef	
F_v'/F_m'	PSII maximum ef	photochemistry at a given PPFD, which is the PSII operating efficiency if all the PSII centers were 'open' (Q_A oxidized).
F_q'/F_v'	PSII efficiency factor	Relates the PSII maximum efficiency to the PSII operating efficiency. Nonlinearly related to the proportion of PSII centers that are 'open' (Q_A oxidized). Mathematically identical to the coefficient of photochemical quenching, q_P.
NPQ	Nonphotochemical quenching	Estimates the nonphotochemical quenching from F_m to F_m'. Monitors the apparent rate constant for heat loss from PSII. Calculated from $(F_m/F_m') - 1$.
q_E	Energy-dependent quenching	Associated with light-induced proton transport into the thylakoid lumen. Regulates the rate of excitation of PSII reaction centers.
q_I	Photoinhibitory quenching	Results from photoinhibition of PSII photochemistry.
q_L	Fraction of PSII centers that are 'open'	Estimates the fraction of 'open' PSII centers (with Q_A oxidized) on the basis of a lake model for the PSII photosynthetic apparatus. Given by $(F_q'/F_v')(F_o'/F')$
q_T	Quenching associated with a state transition	Results from phosphorylation of light-harvesting complexes associated with PSII
ϕ_F	Quantum yield of fluorescence	Number of fluorescent events for each photon absorbed

Baker N.R. (2008), Chlorophyll fluorescence: a probe of photosynthesis *in vivo*. Ann. Rev Plant Biol 59: 89-113

Early fluorescence imaging experiment

Kautsky and Hirsch (1931) irradiated a dark-adapted leaf with a blue light and observed it visually through a dark-red glass. Here is a high-tech presentation of what they saw:

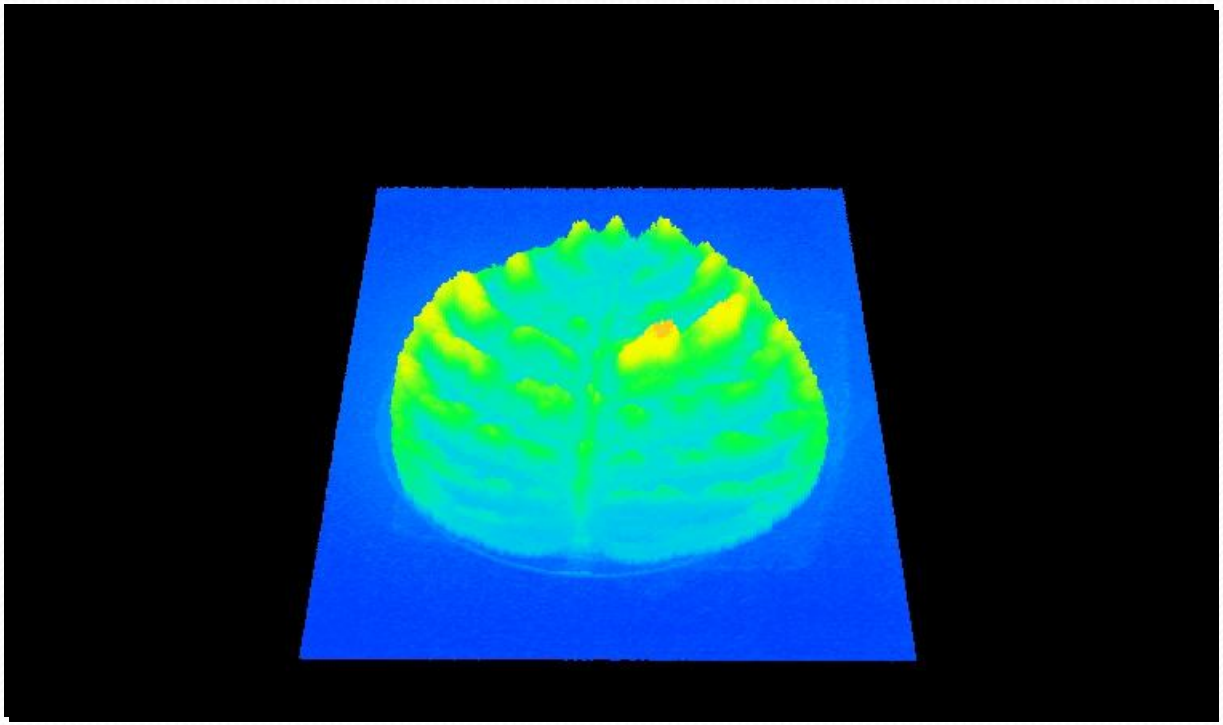

Heterogeneity revealed by imaging

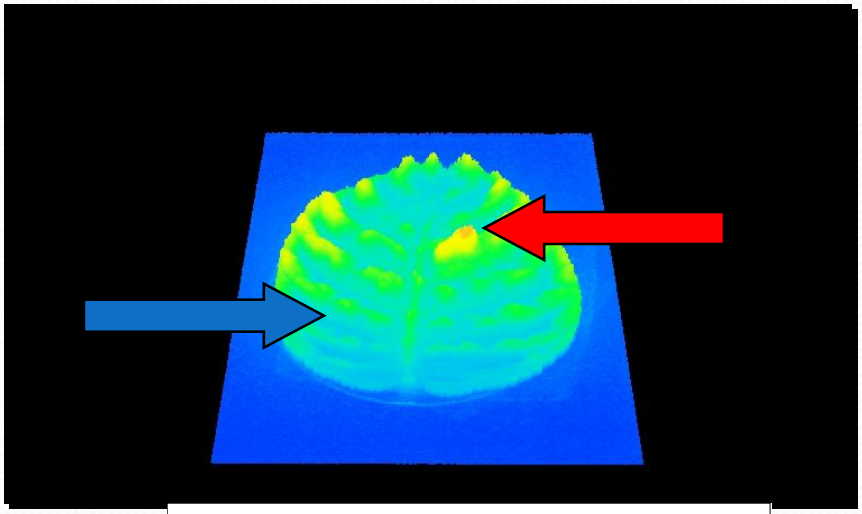

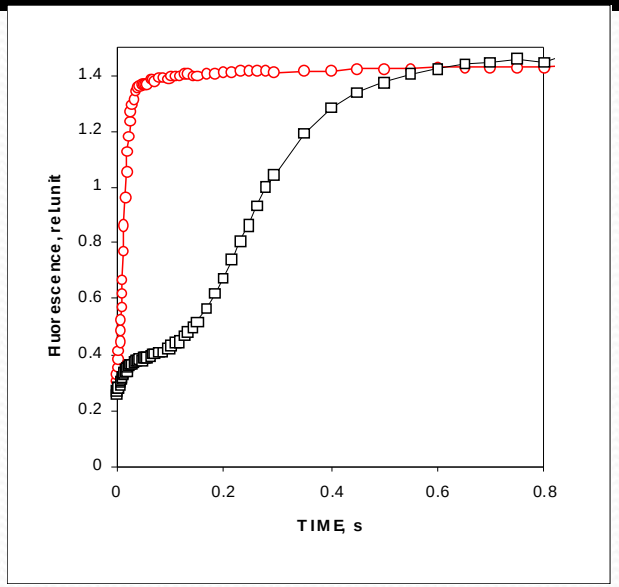

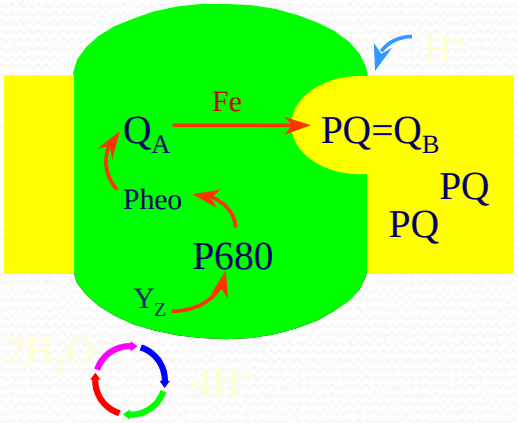

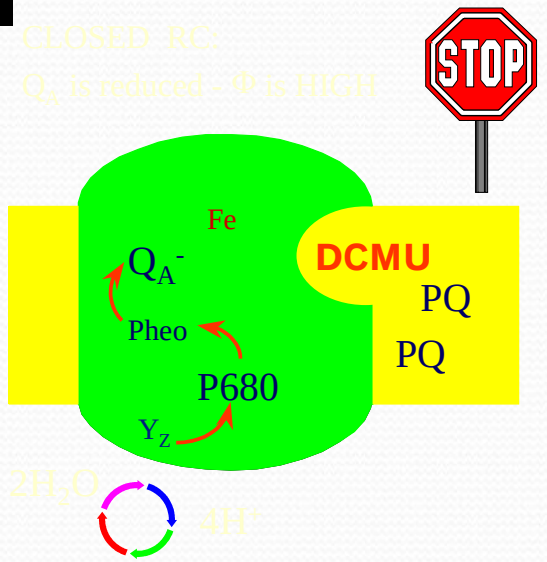

Structured light [3D + Chl-F]$_{(t)}$ imaging

Bellasio, C., Olejníčková, J., Tesař, R., Šebela, D. & Nedbal, L. (2012).
Computer Reconstruction of Plant Growth and Chlorophyll Fluorescence Emission in Three Spatial Dimensions. Sensors 2012, 12: 1052-1071

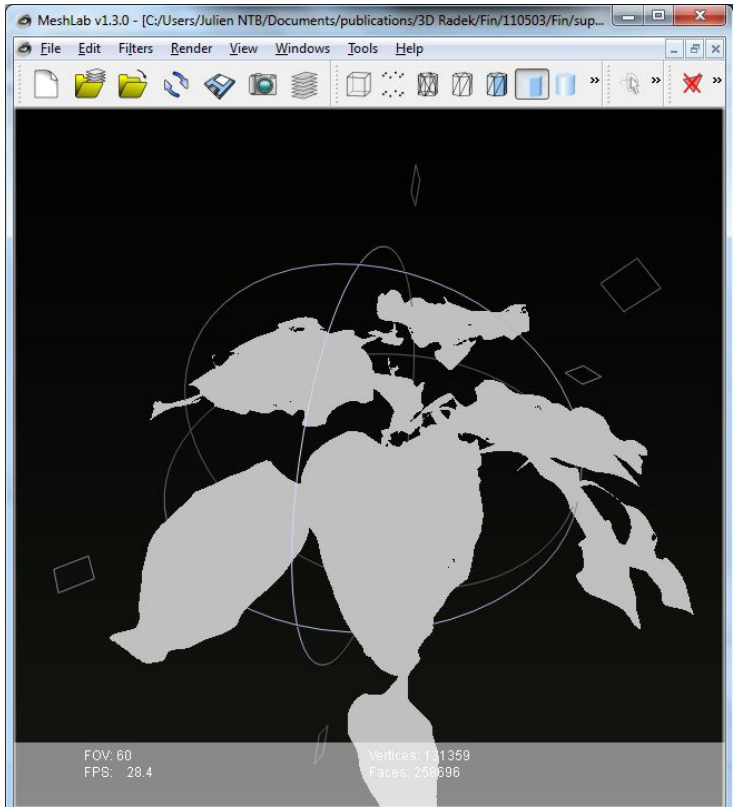

meshlab.sourceforge.net/

Figure 9. Distribution of Rfd100 parameter over water stressed pepper plants

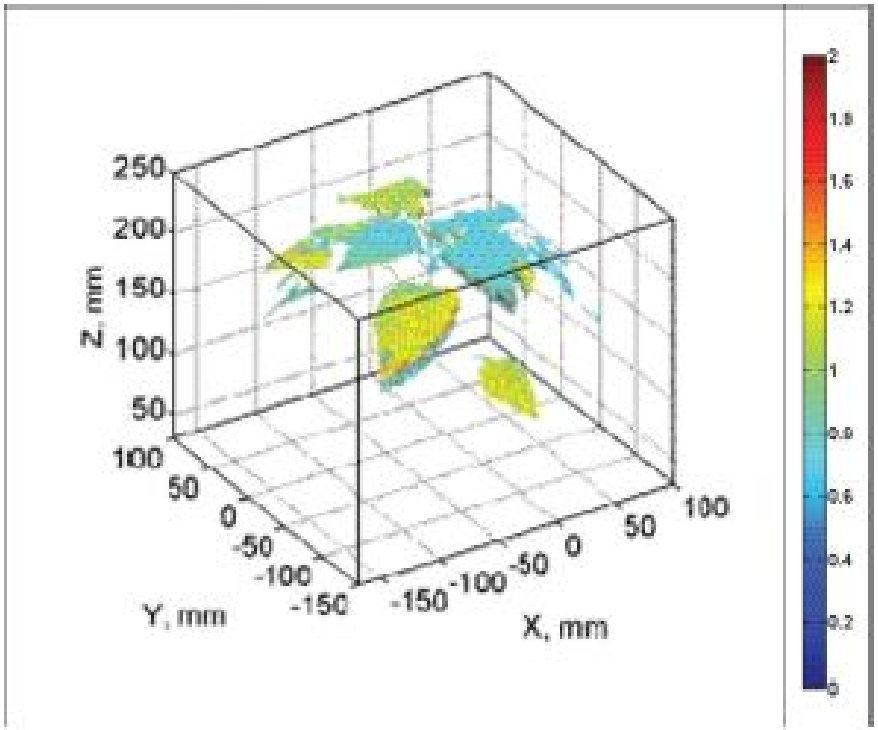

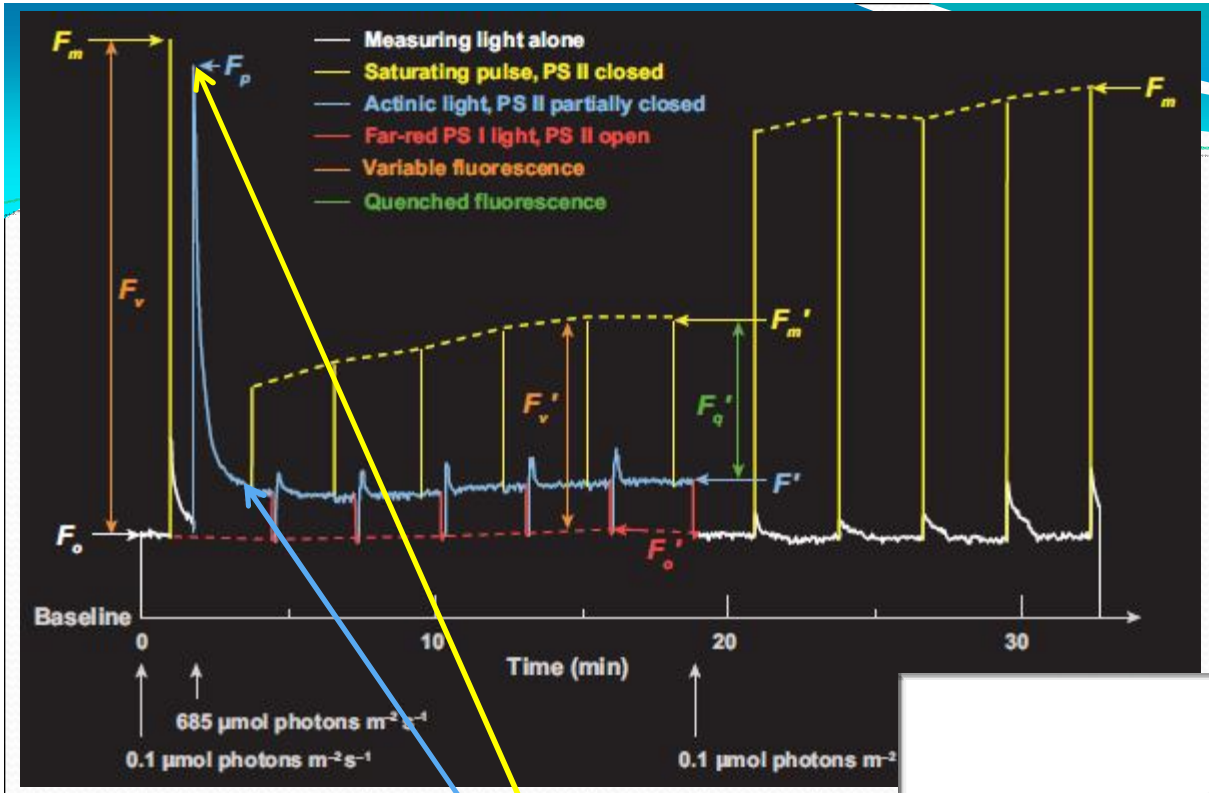

fluorescence decrease ratio
RFd= (Fp-F')/Fp

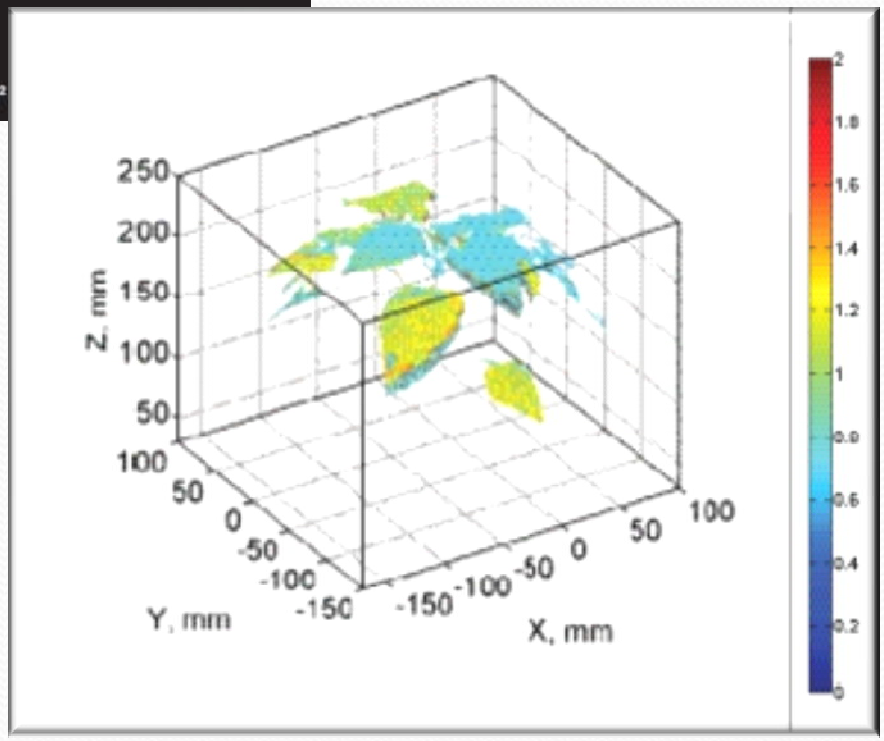

Baker N.R. (2008), Chlorophyll fluorescence: a probe of photosynthesis *in vivo*. Ann. Rev Plant Biol 59: 89-113

Lichtenthaler, H.K., Buschmann, C., Rinderle, U., and Schmuck, G. 1986, Radiat. Environ. Biophys., 25, 297.

1. Plant 3-D reconstruction
2. Adding Chl-fluorescence in time to 5-D
3. Statistical feature selection and combinatorial imaging

What images in the sequence carry the information?

Fiorani and Schurr (2013) Annu. Rev. Plant Biol.64:17.1–17.25

Cost reductions and time gains are desirable targets when designing phenotyping at a large scale (9). First, researchers need sound and robust knowledge about the phenes that are indicative of the intended performance. Here, mechanistic understanding and deep phenotyping play a key role in identifying useful parameters and proxies to measure. It is clearly valuable to identify a set of parameters before wasting resources by measuring a large number of data points, which could be highly autocorrelated or not indicative of the target performance.

Imaging regulatory response during pathogen-host interaction

Host-pathogen:

Model plant:
Arabidopis thaliana

Model pathogen:
Pseudomonas syringae

External stimulation by light:

Differential dynamic resonse of healthy and infected tissue to external stimulation was expected
Here, 14 different dynamic light patterns of one of two types were employed and tested:
2 patterns of Kautsky effect protocol type [1] and 12 patterns of harmonic forcing protocol type [2]

[1]

Stimulation by irradiance(t)

[2]

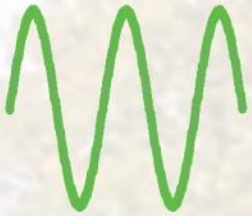

Fig.1A Plant leaf 24 hours after inoculation by bacteria. No visible symptoms.

Output Fluo(t)

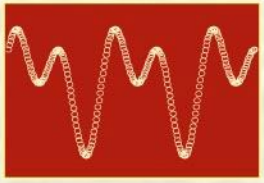

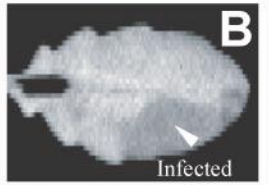

Fig.1B Plant leaf fluorescence, Fm during saturating flash of light, 24 dpi

Which images yield the highest contrast?

Fig.3 The contrast between healthy and infected leaf segments is different in different images

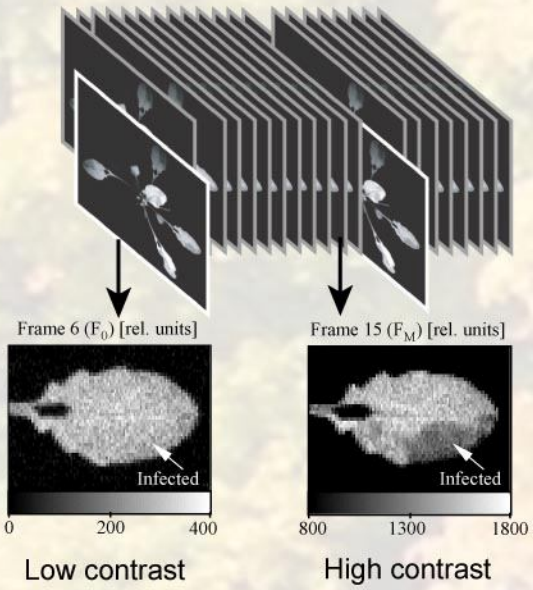

Fig.4 The leaf is divided into two halves:

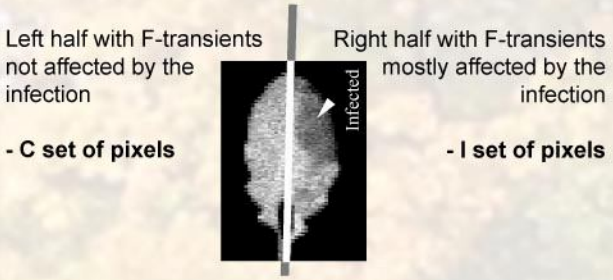

Fig.5 A subset of n images is evaluated for contrast, i.e. for its capacity to discriminate between the healthy and infected leaf segments.

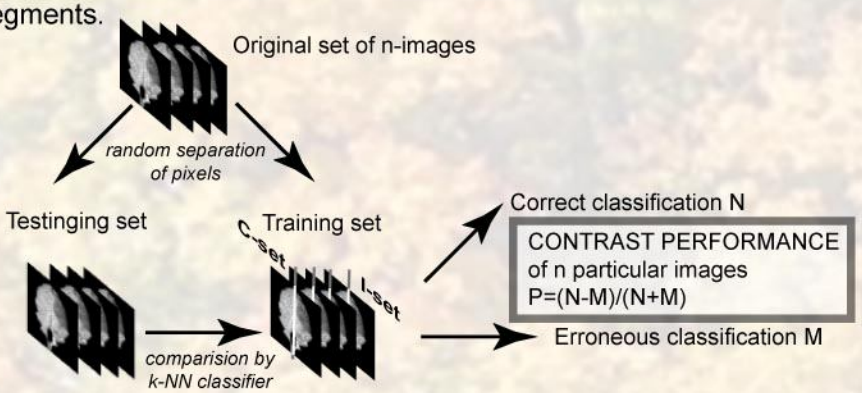

Sequentional Forward Floating Selection (SFFS)

Fig.5 The objective of the algorithm [4] was to identify a set of n images, that yield the highest contrast between the healthy and infected tissue segments. The contrast was determined by the performance of n images as defined in panel 4. The typical number of images considered in classification was 3. Further increase of this number led to only limited increase in performance (not shown). The figure shows schematically the SFFS algorithm.

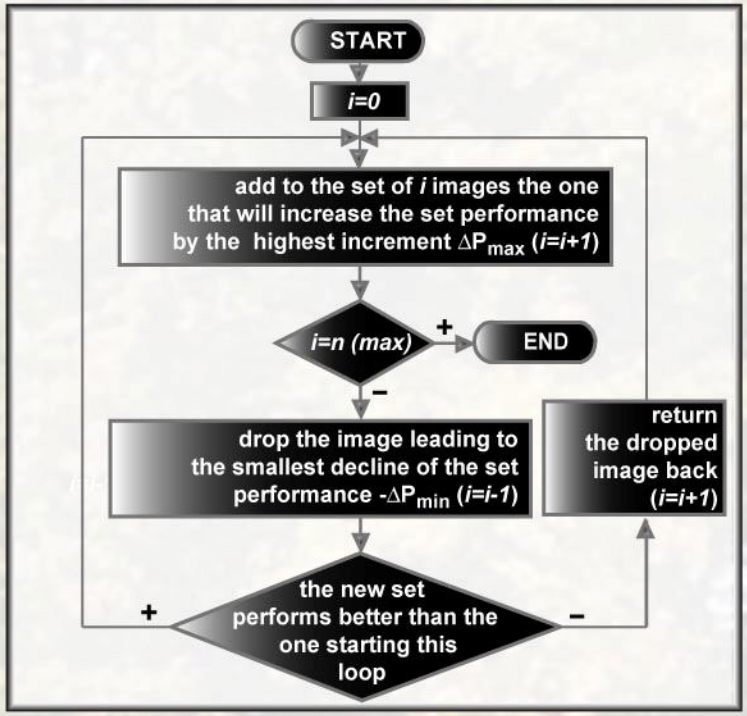

Contrast in individual F-imaging protocol blocks

Tab.1. Classification performance reflects the contrast between infected and healthy tissue segments in sets of 3 images selected from individual protocol blocks with k-NN classifier (k=5). Light in the first column represents the irradiance amplitude in µmol(photons).$m^{-2}.s^{-1}$ that is characteristic for the respective protocol block. Compare the performance of the individual protocol blocks with the performance of 0.9 that was achieved with the complete protocol (framed top row). The level of performance is indicated by the background shading.
The image ID in the third column identifies the phase of the Kautsky protocol in which the relevant image was taken or gives the serial number of the respective image. In the case of harmonic forcing, the relevant image shows phase (F) or amplitude (A) of the 1st, 2nd or 3rd harmonics and the mean emission yield (A0).

LIGHT µmol(photons).$m^{-2}.s^{-1}$	STIMULATION PROTOCOL DESCRIPTION	IMAGE SET	IMAGE SET PERFORMANCE (HEALTHY-INFECTED CONTRAST)
80,80,160	All protocols combined	F1 T=12s, T=48s, T=24s	0.90
0	F0, FM, dark relaxation	2xF0,FM	0.50
50	Kautsky effect without quenching	FP,56,62	0.58
50	Quenching analysis during Kautsky	41,FM1,FM2	0.48
0	Dark relaxation after Kautsky	FM3,FM4,F0'	0.42
200	Kautsky effect in without quenching	FP,168,172	0.42
200	Quenching analysis during Kautsky	2x FM1,FM2	0.34
0	Dark relaxation after Kautsky	FM3,FM4,F0'	0.30
80	Harmonic forcing with T=1.5s	F1,F2,F3	0.30
80	Harmonic forcing with T=3s	F1,F2,A3	0.34
80	Harmonic forcing with T=6s	F1,F2,A2	0.36
80	Harmonic forcing with T=12s	F1,F3,A3	0.58
80	Harmonic forcing with T=24s	F1,F2,F3	0.70
80	Harmonic forcing with T=48s	F1,F2,F3	0.76
160	Harmonic forcing with T=1.5s	F1,F2,F3	0.28
160	Harmonic forcing with T=3s	F1,F2,F3	0.42
160	Harmonic forcing with T=6s	F1,F2,F3	0.46
160	Harmonic forcing with T=12s	F1,F2,F3	0.68
160	Harmonic forcing with T=24s	F1,F2,F3	0.64
160	Harmonic forcing with T=48s	F1,F2,F3	0.60

SFFS identifies image combinations that can detect an early response to biotic stress

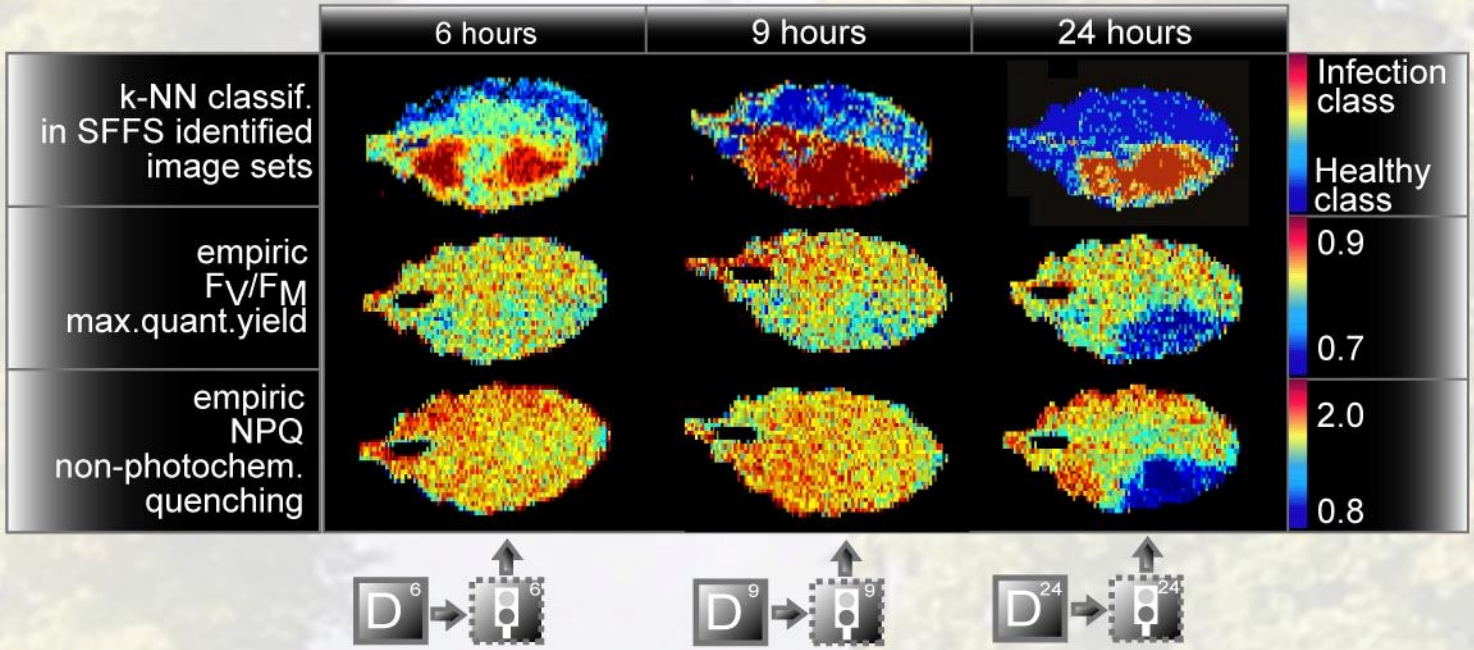

Fig.6 The figure documents that image sets identified by the SFFS algorithm and the corresponding training sets from infected and healthy tissue segments can be used to visualize the progress of infection with contrast (top row) that is by far superior over the empiric parameters dominantly used so far (two bottom rows). The false colors in the top row show relative distance to the respective training sets. Red indicates proximity to the I (infected) set, blue represents pixels closer to the C (control) healthy tissue set.

The newly identified dynamic features can distinguish early and late phase of the infection

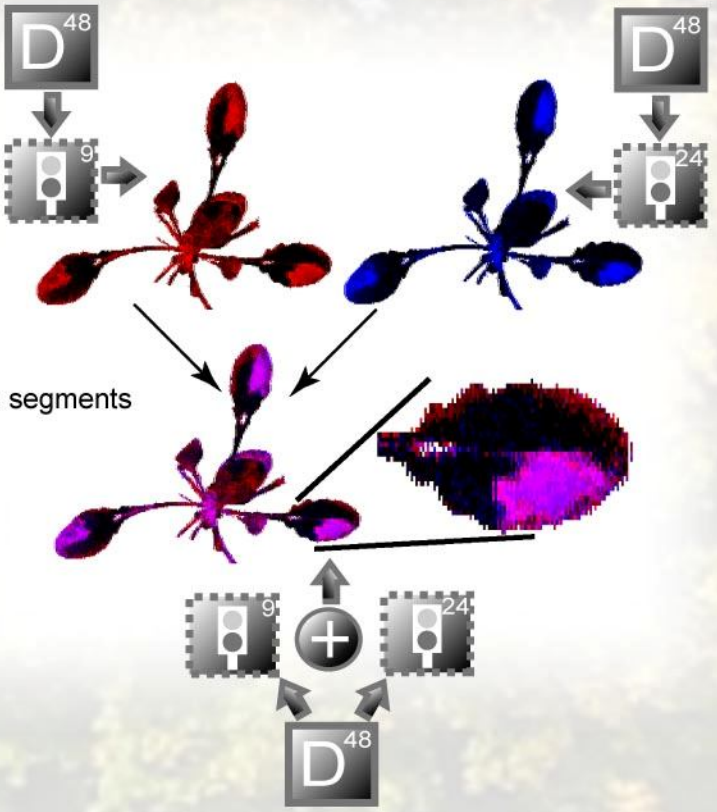

Fig.7 The training sets from plants 9 and 24 hours after the infection were used as signatures of the early and late phase of the infection. Pixel signals captured with a plant 48 hours after the infection were investigated for their distance to the 9 and 24 hours infection signatures (top images). Red shows distance to the early infection signature and blue to the late phase infection signature. The early and late infection segments overlap but are not identical. The bottom image with the detail view combine the blue and red into one RGB image. The red edge in the image shows the early phase advancing wave of the infection whereas the violet and blue center represents the late phase infection core approaching necrosis.